Assessment of the Potential Role of *Streptomyces* in Cave Moonmilk Formation

Marta Maciejewska[1], Delphine Adam[1], Aymeric Naômé[1], Loïc Martinet[1], Elodie Tenconi[1], Magdalena Całusińska[2], Philippe Delfosse[2], Marc Hanikenne[3,4], Denis Baurain[4,5], Philippe Compère[6], Monique Carnol[7], Hazel Barton[8], and Sébastien Rigali[1*]

[1]InBioS - Centre for Protein Engineering, Institut de Chimie B6a, University of Liège, B-4000, Liège, Belgium

[2]Environmental Research and Innovation Department, Luxembourg Institute of Science and Technology, Rue du Brill 41, Belvaux, L-4422, Luxembourg

[3]InBioS - Functional Genomics and Plant Molecular Imaging, University of Liège, B-4000 Liège, Belgium

[4]PhytoSYSTEMS, University of Liège, B-4000 Liège, Belgium

[5]InBioS – Eukaryotic Phylogenomics, University of Liège, B-4000, Liège, Belgium

[6]Department of Biology, Ecology and Evolution & Centre of Aid for Research and Education in Microscopy (CAREm-ULg), Institute of Chemistry B6a University of Liège, B-4000, Liège, Belgium

[7]InBioS - Plant and Microbial Ecology, Botany B22, University of Liège, B-4000, Liège, Belgium

[8]Department of Biology, University of Akron, Akron, Ohio, United States of America

[*]Corresponding author. E-mail: srigali@ulg.ac.be; Tel: +32 4 366 98 30; Fax: +32 4 366 33 64

Keywords: biomineralization, moonmilk genesis, geomicrobiology, carbonatogenesis, cave microbiology

Abstract

Moonmilk is a karstic speleothem mainly composed of fine calcium carbonate crystals ($CaCO_3$) with different textures ranging from pasty to hard, in which the contribution of biotic rock-building processes is presumed to involve indigenous microorganisms. The real bacterial input in the genesis of moonmilk is difficult to assess leading to controversial hypotheses explaining the origins and the mechanisms (biotic versus abiotic) involved. In this work we undertook a comprehensive approach in order to assess the potential role of filamentous bacteria, particularly a collection of moonmilk-originating *Streptomyces*, in the genesis of this speleothem. Scanning electron microscopy (SEM) confirmed that indigenous filamentous bacteria could indeed participate in moonmilk development by serving as nucleation sites for $CaCO_3$ deposition. The metabolic activities involved in $CaCO_3$ transformation were furthermore assessed *in vitro* among the collection of moonmilk *Streptomyces*, which revealed that peptides/amino acids ammonification, and to a lesser extend ureolysis, could be privileged metabolic pathways participating in carbonate precipitation by increasing the pH of the bacterial environment. Additionally, *in silico* search for the genes involved in biomineralization processes including ureolysis, dissimilatory nitrate reduction to ammonia, active calcium ion transport, and reversible hydration of CO_2 allowed to identify genetic predispositions for carbonate precipitation in *Streptomyces*. Finally, their biomineralization abilities were confirmed by environmental SEM, which allowed to visualize the formation of abundant mineral deposits under laboratory conditions. Overall, our study provides novel evidences that filamentous Actinobacteria could be key protagonists in the genesis of moonmilk through a wide spectrum of biomineralization processes.

Introduction

The hypogean environment, although highly deprived of nutrients, sustains a diverse microbial life. This subterranean microbiome plays an important ecological role in caves, with secondary effects on mineralogy, including host rock dissolution or mineral precipitation, leading to the formation of various secondary mineral deposits termed speleothems (Barton and Northup 2007; Jones 2010; Cuezva et al. 2012). A biogenic origin has been hypothesized for a number of speleothems, including coralloids (Banks et al. 2010), pool fingers (Melim et al. 2001), ferromanganese deposits (Northup et al. 2003; Spilde et al. 2005), helictites (Tisato et al. 2015), and moonmilk (Cañaveras et al. 2006). Unlike typical mineral deposits, moonmilk is present as a soft and pasty precipitate on cave surfaces and within pools (Richter et al. 2008; Cacchio et al. 2014). The origin of moonmilk has been controversial for many years due to the complex mineralogy, the atypical crystalline morphology, and also the size of its crystals (Verrecchia and Verrecchia 1994; Cañaveras et al. 1999; Cañaveras et al. 2006; Bindschedler et al. 2010; Bindschedler et al. 2014). Notably, moonmilk deposits are characterized by several crystal habits including nano-fibers, and micro-meter sized needle-fiber crystals in a form of monocrystalline rods and polycrystalline chains (Cañaveras et al. 1999; Cañaveras et al. 2006; Bindschedler et al. 2010; Bindschedler et al. 2014). While initially postulated as a speleothem of abiotic origin (Harmon et al. 1983; Borsato et al. 2000), recent studies attributed the genesis of moonmilk to indigenous microbial population (Cañaveras et al. 2006; Cailleau et al. 2009; Baskar et al. 2011; Braissant et al. 2012).

Microbial carbonate precipitation (MCP) is a broad spectrum phenomenon either mediated by autotrophic pathways, such as photosynthesis and methanogenesis that lead to depletion of local

CO_2, or heterotrophic pathways that alter local conditions to promote $CaCO_3$ precipitation (Castanier et al. 2000; Banks et al. 2010). Caves are devoid of sunlight, ruling out photosynthesis, while methanogenesis has been documented rarely in these systems. Heterotrophic processes may therefore play an important role (Banks et al. 2010). Active calcite precipitation by heterotrophs in calcium-rich environments has been hypothesized to be the consequence of a detoxification process, wherein the acidification of the local environment induced by passive influx of Ca requires growing cells that would actively export the excess of this metal to maintain cellular calcium homeostasis (Banks et al. 2010). Such metal detoxification strategies have also been linked to the formation of the unusual speleothems known as helictites (Tisato et al. 2015). Heterotrophic growth can also increase the environmental pH, which can in turn increase the saturation index of $CaCO_3$ and drive precipitation. Calcite precipitation through nitrogen metabolism is thought to operates by different metabolic pathways, including ureolysis, ammonification through amino acid and peptide catabolism, and dissimilatory nitrate reduction to ammonia (DNRA), all of which increase the local pH (Fig. 1) (Castanier et al. 2000).

Moonmilk was reported to host wide spectrum of microbiota, including Archaea, Bacteria, and Fungi (Rooney et al. 2010; Portillo and Gonzalez 2011; Engel et al. 2013; Reitschuler et al. 2014; Reitschuler et al. 2015; Axenov-Gibanov et al. 2016; Maciejewska et al. 2016; Reitschuler et al. 2016). Among this microbiome, Fungi and filamentous microorganisms, particularly members of Actinobacteria phylum were reported to be possibly involved in the moonmilk genesis (Cañaveras et al. 2006; Bindschedler et al. 2010; Bindschedler et al. 2014). Bindschedler et al. (2010, 2014) suggested that the presence of nano-fibers within the crystalline structure of moonmilk was associated with biomineralized fungal hyphae. The authors suggest that organized networks of nano-fibers, often observed in moonmilk, could represent fibrous fungal cell wall polymers, such as chitin and β-(1→3)glucans (Bindschedler et al. 2010). On the other hand, the

observation of unstructured aggregates of unconsolidated microcrystalline fibers with calcified Actinobacteria-like filaments led Cañaveras et al. (2006) to propose a model of moonmilk formation wherein Actinobacteria promoted calcium carbonate precipitation by creating locally favorable conditions, with the bacterial cell walls serving as nucleation zones (Cañaveras et al. 2006). The presence of metabolically active microorganisms in moonmilk was demonstrated using isothermal microcalorimetry (Braissant et al. 2012), although the progressive accumulation of $CaCO_3$ (and presumably entombment) ultimately leads to a decrease of the microbial activity (Cañaveras et al. 2006; Sanchez-Moral et al. 2012). As a result, microorganisms would play a significant role in the initiation of moonmilk formation, which ultimately would be overtaken by abiotic processes leading to the growth of the deposit, which can reach up to 1 m in thickness (Sanchez-Moral et al. 2012).

In all of these studies, there has been no clear distinction as to whether the increase or decrease in local pH is ultimately leading to the precipitation of moonmilk by the dominant actinobacterial species observed. In this work we use a combination of microscopy, cultivation and genomic approaches to provide an *in vitro* and *in silico* assessment of the actinobacterial metabolic activities that could promote $CaCO_3$ precipitation. Our data suggest that the *Streptomyces* species would play an important role in nitrogen metabolism, which could locally raise pH and contribute to moonmilk formation.

Materials and methods

Moonmilk sampling and *Streptomyces* strains used in this study

Samples for microscopy and cultivation were taken from moonmilk deposits originating from three sampling points (collection points COL1, COL3, COL4, supplementary Fig. 1 from Maciejewska

et al. 2016) in the upper Viséan limestone cave 'Grotte des Collemboles' (Springtails' Cave), Comblain-au-Pont, Belgium (more detailed cave description in supplementary Fig. 1).

Moonmilk samples for strains isolation were brought to the laboratory on ice and stored at 4°C prior to lyophilization. Extensive attempts at the cultivation of Actinobacteria led to the isolation of 31 phylogenetically distinct *Streptomyces* strains representing phylogenetically distinct phylotypes (as previously described in Maciejewska et al. 2016 and supplementary Fig. 2). Moonmilk samples for scanning electron microscopy (SEM) were preserved in two separate fixative solutions, 2.5% glutaraldehyde in 0.1 M Na-acetate buffer (pH 7.4), and 100% ethanol, and stored at 4°C until analysis. To exclude the effect of fixatives on the crystalline structure of moonmilk, the lyophilized samples were also observed under the microscope as controls (data not shown).

Environmental scanning electron microscopy (ESEM) and elemental X-ray energy dispersive microanalysis (EDS)

Glutaraldehyde-fixed moonmilk samples were post-fixed in 1% osmium tetroxide (OsO_4) in distilled water, rinsed and dehydrated through a graded ethanol series (30-100%). Glutaraldehyde-fixed samples and ethanol-preserved samples were then processed by critical point drying, prior to mounting on the glass slides covered by double-side carbon tape together with lyophilized samples. Parts of each sample were mounted to expose the outer surface, a vertical section or fracture made with a scalpel blade. Dry samples were subsequently sputter coated with platinum on Balzers sputtering Unit SCD 030 (Balzers, Lichtenstein).

The production of mineral deposits by isolates MM24 and MM99 following growth in two different culture conditions - calcite precipitation agar (CPA) and modified B-4 medium (more details in $CaCO_3$ precipitation section) was detected from the living bacterial colonies after being air-dried.

Morphological observations were performed by light microscopy (reflected, transmitted and polarized light) using an Olympus Provis AX-70 microscope fitted with a Visicam 5.0 videocamera for image capture. SEM observations were performed in an environmental scanning electron microscope FEI XL30 ESEM-FEG (Eindhoven, The Netherlands). Platinum-coated samples were observed under high vacuum (HV) conditions with the ET-secondary electron (SE) detector at 10 mm working distance and 15 kV accelerating voltage. Air-dried cultures, were observed under low vacuum (LV) conditions (0.4 Torr) with the large field gaseous secondary electron (GSE) detector and the backscattered electron (BSE) detector at 10 mm working distance and 10 and 20 kV accelerating voltage, respectively. As a result of applying two types of detection – GSE and BSE, the contrast of the images due to the surface morphology or due to the atomic number of the elements and the density of minerals could be obtained. Elemental X-ray microanalysis and mapping was carried out using a Bruker silicon drift energy dispersive detector (SDD Quantax 129 eV, Billerica, MA, USA) at 10-20 kV accelerating voltage with the Esprit 1.9 software. Semi-quantitative analyses of the elemental composition were done using the standard-less ZAF method with automatic background subtraction.

Genomic analysis of moonmilk-derived isolates

The genes of interest (see Fig. 1) including those coding for i) the ureolytic system (*ure*), ii) the $Ca^{2+}/2H^{+}$ antiporter system (*chaA*), iii) the nitrate/nitrite reductases (*nar/nas/nir*) with the corresponding transporters (*narK*), and iv) the carbonic anhydrase (CA) together with sulfate transporter in cluster with CA (*sulP*) (Felce and Saier 2005), were retrieved from the genomes of moonmilk *Streptomyces* sequenced at the Luxembourg Institute of Science and Technology, as previously described (Maciejewska et al. 2016). These genes were first identified within the

chromosome of the model *Streptomyces* species – *Streptomyces coelicolor* (Bentley et al. 2002). The designations of the selected genes are listed in supplementary Table 1. Subsequently, genes sequences encoding the corresponding proteins were identified within the genomes of additional 54 reference *Streptomyces* strains (supplementary Table 2) for which completely assembled genomes are available in NCBI FTP server (data retrieved on January 8th 2016).

A total of 407,461 protein sequences were organized in clusters of orthologous groups (COGs) using Proteinortho v 5.12 (Lechner et al. 2010) with the PoFF extension to further discriminate similar sequences based on synteny. Created COGs were used as models to screen moonmilk *Streptomyces* genomes. For every *S. coelicolor* gene, the collection of protein sequences in the corresponding COG was used to build a hidden Markov model (HMM) profile (Eddy 1998). As an example, the gamma sub-unit of the urease metallo-protein of *S. coelicolor* (UreA, SCO1236) clusters in a COG with 52 sequences from other *Streptomyces* (supplementary Table 1). This COG is used to construct a HMM profile representing the UreA protein that is used to search a database of translated predicted coding sequences of the moonmilk *Streptomyces*. Partial coding sequences resulting from the fragmented nature of the moonmilk *Streptomyces* genomes were also considered in the screening. The moonmilk *Streptomyces* coding sequences were predicted with Prodigal v2.6.2 (Hyatt et al. 2010). HMM profile building and HMM search were carried out using the HMMER3 software package (v3.1b2, http://hmmer.org/). The accession numbers of genes recovered from moonmilk *Streptomyces* are compiled in the supplementary Table 3.

Metabolic assays

Ammonification

The ability of isolates to decompose organic nitrogen into ammonia was tested on nutrient agar containing: peptone, 5 g/l; beef extract, 3 g/l; NaCl, 5 g/l; phenol red, 0.012 g/l; agar, 15 g/l; pH

185 7.0 (Food and Agriculture Organization of the United Nations 1983). Each representative
186 moonmilk *Streptomyces* isolate was spot-inoculated on an individual Petri dish and incubated for
187 7 days at 28°C. *Citrobacter freundii* ATCC 43864 was used as a positive control strain, while
188 uninoculated media was used as a negative control. The development of a pink color, indicating a
189 pH increase due to the formation of ammonia following peptides/amino acids degradation was
190 monitored every day during the incubation.
191
192 **Ureolysis**
193 Rapid screening of urease activity was performed on Christensen's Urea Agar Base (UAB) solid
194 media as described previously (Hammad et al. 2013). The UAB medium was prepared as follows:
195 urea, 20.0 g/l; NaCl, 5.0 g/l; peptone, 1.0 g/l; glucose, 1.0 g/l; KH_2PO_4, 2.0 g/l; phenol red, 0.012
196 g/l and agar, 15.0 g/l; pH 6.5. All components of the media were autoclaved except urea which was
197 filter-sterilized and added after autoclaving. The UAB medium without urea was used as a negative
198 control. Both types of media were inoculated with representative of each phylotype together with
199 urease negative control strain (*Escherichia coli* ATCC 25922) and urease positive control strain
200 (*Klebsiella pneumoniae* ATCC 13883) and incubated at 28°C. Plates were examined continually
201 to record development of the pink color indicating a pH increase as a result of urease enzyme
202 activity, leading to generation of ammonia through urea degradation, according to the following
203 reaction: $(NH_2)_2CO + H_2O \rightarrow 2NH_3 + CO_2$.
204
205 **Nitrate and nitrite reduction**
206 The assessment of nitrate and nitrite reduction was performed as described by Li et al. (2016), with
207 small modifications. Briefly, the phylotypes were inoculated in nitrate or nitrite agar slants

(potassium nitrate / sodium nitrite, 1g/l; peptone, 5 g/l; beef extract, 3 g/l; agar, 12 g/l; pH 7.0) and nitrate / nitrite broth tubes (potassium nitrate / sodium nitrite, 1g/l; peptone, 5 g/l; beef extract, 3 g/l; pH 7.0) equipped with the Durham tubes. *Escherichia coli* ATCC 25922 was used as a control strain for exclusive reduction of nitrate to nitrite, while *Pseudomonas aeruginosa* ATCC 27853 as a complete reducer of nitrate into the nitrogen gas, collected in the Durham tube. Uninoculated media were used as an additional control. Inoculated test tubes were incubated at 28°C for 9 days in static conditions, to reduce amount of dissolved oxygen. After incubation time few drops of sulfanilic acid and alpha-naphthylamine were added to each test tube, which together react with nitrite generating red/pink color. Reduction of nitrate (NO_3^-) is indicated by appearance of red color in nitrate broth, while red color disappearance in nitrite broth indicates nitrite (NO_2^-) reduction.

Oxidative glucose breakdown

The glucose oxidative test was carried out according to Hugh and Leifson (1953). Briefly, each representative of the phylotypes was spot-inoculated on Hugh and Leifson's OF basal medium, prepared as follows: peptone, 2.0 g/l; NaCl, 5.0 g/l; bromothymol blue, 0.03 g/l; K_2HPO_4, 0.3 g/l; agar, 3.0 g/l; pH 7.1. Filter-sterilized glucose was added after autoclaving to a final concentration of 1%. The OF medium not supplemented with glucose was used as a negative control, and oxidative *Pseudomonas aeruginosa* ATCC 27853 strain as a positive control. The inoculated plates were incubated at 28°C during 7 days and monitored continually to observe development of yellow color indicating on the acid production due to glucose metabolism.

$CaCO_3$ precipitation

The screening for isolates able to precipitate calcium carbonate through ureolysis was performed using calcite precipitation agar (CPA) as previously described (Stocks-Fischer et al. 1999). The

CPA medium was prepared as follows: (g/l); nutrient broth, 3.0 g/l; urea, 20.0 g/l; $CaCl_2*2H_2O$, 28.5 g/l; $NaHCO_3$, 2.12 g/l; NH_4Cl, 10.0 g/l; Agar, 15.0 g/l. All components were autoclaved apart from urea, which was added filter-sterilized. The same medium, but without urea, was used as an additional control. Alternatively, precipitation of $CaCO_3$ was tested on modified B-4 medium (pH 7.0) composed of: yeast extract, 4 g/l; calcium acetate, 2.5 g/l; agar, 15 g/l. The plates inoculated with MM24 and MM99, following incubation at 28°C, were examined under ESEM after 2 months of incubation for CPA media, and 1 month of incubation for B-4.

$CaCO_3$ solubilization

Isolates were tested for their ability to solubilize calcium carbonate on two different media including i) minimal medium (MM) (Kieser et al. 2000) containing $CaCO_3$ (2 g/l), supplemented or not with glucose (5 g/l), and ii) 1:100 diluted nutrient agar (Portillo et al. 2009), containing $CaCO_3$ (2.5 g/l), supplemented or not with glucose (2 g/l). The spot-inoculated plates were incubated for 4 weeks at 28°C and the capability of calcium carbonate solubilization was confirmed by observation of the clear halo around a colony.

Results ~~and Discussion~~

Microscopic evaluation of indigenous moonmilk filamentous bacteria as nucleation sites for carbonate precipitation

Filamentous bacteria, particularly Actinobacteria, have been proposed to participate in the genesis of moonmilk deposits by serving as nucleation sites for carbonate deposition (Cañaveras et al. 2006). Regardless the fixation procedure (glutaraldehyde, ethanol, and freeze-drying),

classical SEM observations revealed the same crystal morphologies that have also been described in the literature (data not shown) (Cañaveras et al. 1999; Cañaveras et al. 2006; Bindschedler et al. 2010; Bindschedler et al. 2014). The surface of moonmilk samples revealed the presence of dense, unstructured meshes of micrometer-size filaments known as needle-fiber calcite (Fig. 2a), which, based on EDS analysis, were shown to be mainly composed of calcium, carbon and oxygen (supplementary Fig. 3a). The structure of moonmilk deposits was characterized by the presence of abundant, randomly oriented, monocrystalline rods and polycrystalline fibers composed of stacked rhombohedra (Fig. 2a). Those crystals showed variable dimensions, ranging from 0.5 – 1 µm width and 30 - 100 µm length for monocrystals, and 2 - 20 µm width, 10 - 100 µm length for polycrystals, as previously reported (Cañaveras et al. 1999). Interestingly, we observed within the moonmilk microscopic composition, abundant networks of filaments with nano-sized width (50 - 150 nm), which either formed compacted pellets (Fig. 2b) or mats (Fig. 2c). The organized networks of nano-fibers, similar to the one observed in Fig. 2c, were previously reported from moonmilk and associated with fungal wall polymers (Bindschedler et al. 2010; Bindschedler et al. 2014). However, randomly-oriented, compacted pellets of nano-fibers as presented on Fig. 2b, were highly comparable to Actinobacteria, but characterized by a much smaller cell size which could be a result of the oligotrophic nature of the cave environment. It has been demonstrated that the cell size is largely dependent on the nutritional status of the environment, with resource-poor ecosystems stimulating dwarfism (Young 2006; Portillo et al. 2013). In this work, the observed size of the putative bacterial nano-filaments, ranging from 0.05 to 0.15 µm, could also be a consequence of the oligotrophic nature of the moonmilk niche as cell elongation/filamentation has been shown to be the result of nutritional stress in some bacteria (Steinberger et al. 2002), including Actinobacteria (Pine and Boone 1967; Wills and Chan 1978; Deutch and Perera 1992). However, even in nutrient-rich soils the majority of bacteria can display a diameter less than 0.2 µm (Hahn 2004). In addition,

the imprints of nano-sized microorganisms were already reported from other geological formations, such as sedimentary rocks (Folk and Chafetz 2000; Folk 1993). Finally, recent findings of ultra-small marine Actinobacteria with an average diameter of about 0.3 µm, provides an additional evidence for the existence of nano-bacteria in oligotrophic ecosystems (Ghai et al. 2013). Unlike crystal fibers, the tiny filaments observed in glutaraldehyde- and ethanol-fixed samples, were not completely straight and regular in their shape but rather displayed plasticity and were often curved, either without preferential orientation (Fig. 2b) or in the same direction (Fig. 2d/e). The tiny, curved filaments were not observed - probably not preserved - in freeze-dried samples that suffered of ice crystal growth (data not shown). One-directional growth is not a typical behavior of growing actinobacterial filaments that are commonly branching in diverse directions in order to form a complex mycelial network. This rigid and unidirectional growth might suggest that they represent calcified filaments potentially still actively growing at their tip, which remains curved (Fig. 2d). Elemental analysis performed with EDS revealed that the observed nano-size filaments contained higher content of carbon and oxygen in comparison to the surrounding crystals, suggesting a possible biological origin (supplementary Fig. 3b). However, these EDS analyses should be viewed with great prudence as the difference in the elemental compositions between filaments and crystals could simply be a consequence of the structure and not the nature (organic vs mineral) of the analyzed areas. Additionally, along (Fig. 2f) or on the tip (Fig. 2g) of some filaments, a possible initiation of calcium carbonate deposition was observed. Besides nano-sized filaments, reticulated filaments were sporadically observed within moonmilk crystals (Fig. 2h). Those particular filamentous forms, with the size of about 0.5 µm width and up to 75 µm length, are often found in subsurface environment, including limestone or lava caves, and possess higher carbon content than the one typically observed for calcite minerals, suggesting their biogenic origin. However, the associated microorganisms are not yet identified (Melim et al. 2008; Northup et al. 2011; Miller et

al. 2012; Melim et al. 2015). Overall, these observations tend to confirm the hypothesis of filamentous microorganisms (bacteria and fungi) serving as a nucleation sites for moonmilk mineral deposition (Cañaveras et al. 2006; Bindschedler et al. 2010; Bindschedler et al. 2014).

Potential role of cultivable moonmilk-derived *Streptomyces* in carbonate precipitation

A nucleation site itself is not sufficient to promote $CaCO_3$ precipitation, as dead bacterial cells lose the ability to precipitate minerals (Banks et al. 2010). The dominant role of bacteria in calcification is attributed to metabolic activities which increase the pH of the environment (above pH 8) and therefore favor a shift of the $CO_2 – HCO_3^- – CO_3^{2-}$ equilibrium towards carbonate ions which precipitate with Ca^{2+} ions. We screened 31 representative *Streptomyces* strains isolated from moonmilk (see supplementary Fig. 2 retrieved from Maciejewska et al. 2016) for their metabolic activities that could lead to a raise in pH, including ureolysis, peptides/amino acids ammonification, and dissimilatory nitrate/nitrite reduction to ammonia (Fig. 1). Although these assays were performed under laboratory conditions, a qualitative assessment of these processes allowed ranking the tested phylotype representatives according to their metabolic performance, and therefore their potential to drive biomineralization through an increase in the extracellular pH. The results are shown in Fig. 3, along with a compilation of activities and phylogenetic relationships (Fig. 4). The results of each metabolic activity assay for all the tested strains are presented in supplementary Fig. 4.

Ureolysis

Among the 31 isolates tested, 15 showed an ability to increase the pH by hydrolysis of urea (Fig. 4). MM99 and MM122 were the strongest ureolytic strains, with comparable metabolic performance to the positive control strain - *Klebsiella pneumoniae* ATCC 13883 (Fig. 3a and supplementary Fig. 4a). The majority of urease-positive moonmilk isolates displayed weak and moderate activities, which were observed either within 3 days of incubation (5 strains) or after extended time (more than 1 week) (6 strains) (Fig. 3a and supplementary Fig. 4a).

In order to know if a relation could be established between the assessed *in vitro* activity and the genetic predispositions for ureolysis, we examined the genomes of the phylotype representatives for the presence of urease genes. We used HMM profiles constructed from Clusters of Orthologous Groups (COGs) of proteins of the urease structural subunits (UreA/UreB/Ure(AB)/UreC), as well as the accessory proteins (UreF/UreG/UreD). The corresponding genes originate from functional clusters of three types *i.e.*, *ureABCFGD, ure(AB)C,* and *ure(AB)CFGD,* which are all present in the urease-positive species. The large majority of moonmilk strains (90%) was found to encode all the urease genes, in some cases present in several copies (Table 1), suggesting that even the strains displaying urease-negative phenotypes are capable of urease activity. This suggests that in urease-negative strains urease activity is not expressed under the conditions tested, or that they harbor mutations that prevent expression or activity. Nonetheless, urea transport appears to be functional in all urease-negative isolates as urea exerted a toxic effect in the growth media of these strains (an effect that could be reversed by growth in the same medium lacking urea; data not shown).

Urease activity has been recently linked to an activity of the zinc-containing enzyme – carbonic anhydrase (CA) (Achal and Pan 2011). While urease maintains an alkaline environment by generating ammonia, carbonic anhydrase would provide carbon dioxide for biomineralization

346 through dehydration of carbonic acid (H_2CO_3) also produced during ureolysis (Fig. 1). It was
347 recently demonstrated that the activities of CA and urease were correlated along the bacterial
348 growth and corresponded to maximum calcite production (Banks et al. 2010; Achal and Pan 2011),
349 while inhibition of carbonic anhydrase activity decreased the rate of calcification, with calcite
350 precipitation occurring more efficiently with the synergistic action of both enzymes – CA and
351 urease (Dhami et al. 2014).

352 The presence of this highly efficient enzyme in cave settings was previously confirmed
353 through metagenomic study of a speleothem in Tjuv-Ante's Cave (Sweden) (Mendoza et al. 2016),
354 and highly acidic cave biofilms, known as 'snottites' (Jones et al. 2011). However, it has never
355 been directly associated to a specific taxonomic group through genome-based approach. The only
356 link was suggested by Cuezva et al. (2012), who proposed CA to be responsible for CO_2
357 sequestration by grey spot colonization found on the walls of Altamira cave, which were dominated
358 by Actinobacteria.

359 Evaluation of the genomes of moonmilk phylotypes for the presence of β-CA (Smith and
360 Ferry 2000), together with the sulfate transporter family protein in cluster with CA (SulP-type
361 permease) revealed that all the investigated strains encode at least one copy of carbonic anhydrase
362 (100% strains encoded β-CA (1) and 87% β-CA (2)) and 90% of them possessing sulfate
363 transporter (Table 1). High copy number of this intracellular zinc metalloenzyme, reaching up to 7
364 copies in MM17, revealed their ubiquitous distribution among karstic bacteria, and suggests their
365 applications in multiple and essential cellular processes beyond their presumed role in carbonate
366 precipitation. Interestingly, a high representation of sulfate permeases of SulP family was also
367 characteristic for the studied population. These broad specificity inorganic anion transporters were
368 suggested to assist bicarbonate (HCO_3^-) transport (Felce and Saier 2005), which was

experimentally confirmed in marine cyanobacteria (Price et al. 2004). While in cyanobacteria SulP transporter mediates HCO_3^-/Na^{2+} symport, the substrate specificity in the case of *Streptomyces* is highly speculative. Nevertheless, fusion of this protein with carbonic anhydrases indeed strongly suggests its participation in HCO_3^- transport. However, whether it is an importer or exporter remains an open question. It could be possible that HCO_3^- uptake through SulP increases the intracellular pool of this inorganic carbon species, which potentially might be efficiently transformed into carbon dioxide by carbonic anhydrases, and be exported outside the cell, unless required for cellular metabolism. Alternatively, SulP-dependent export of intracellularly formed HCO_3^- through CA-mediated hydration of carbon dioxide, would be assisted with import of other ions (Fig. 1). Altogether, these findings reveal abundant distribution of genes involved in the inorganic ionic transport and metabolism, which might be related to the biomineralization phenomenon.

Ammonification

Moonmilk *Streptomyces* were also evaluated for their ability to raise the pH through peptide/amino acid mineralization. 94 % of tested strains efficiently decomposed nitrogenous compounds into ammonia (Fig. 1, Fig. 3b, Fig. 4 and supplementary Fig. 4b). The majority displayed a strong metabolic phenotype (Fig. 5), which is unsurprising given that *Streptomyces* are well known ammonifying bacteria in soils, where they actively participate in the decomposition of organic matter (Prakash et al. 2012). In the isolated cave environment, with limited organic matter input from the surface, the source of such macromolecules is unclear, although peptides and amino acids might be entering the cave through water that has percolated through the soil, making such

391 molecules more readily available than urea (Northup and Lavoie 2001). Amino acid/peptide
392 ammonification was found to be more widespread among the moonmilk isolates than ureolysis,
393 supporting this hypothesis.

394

395 **Dissimilatory nitrate reduction to ammonium**

396 Dissimilatory nitrate reduction to ammonium (DNRA) is another nitrogen cycle-related process
397 considered to be involved in calcification (Castanier et al. 2000) (Fig. 1). This pathway operates in
398 oxygen-limited environments, which could be encountered in the inner layers of the moonmilk
399 deposits. Moreover, moonmilk develops alongside dripping water and its often pasty structure can
400 become fluid, based on its water content, which can drastically reduce oxygen availability.
401 Although *Streptomyces* are obligate aerobes, they are genetically capable of survival under oxygen-
402 limited conditions, encoding genes related to anaerobic respiration, the so-called "anaerobic
403 paradox" (Borodina et al. 2005). Indeed, the model species *Streptomyces coelicolor* was reported
404 to anaerobically respire nitrate (Fischer et al. 2010; Fischer et al. 2014). Though nitrite, the product
405 of this process, was not reduced to ammonia, but detoxified through extrusion via NO_3^-/NO_2^-
406 antiporter system (Fischer et al. 2010; Fischer et al. 2012). In *S. coelicolor* the NirBD reductase
407 was demonstrated to participate in nitrogen assimilation; however a *nirBD* null-mutant grown in
408 the presence of nitrite and excess ammonium was still able to reduce nitrite suggesting the activity
409 of an alternative and yet unknown enzyme (Fischer et al. 2012). We therefore questioned whether
410 moonmilk isolates would be able to mediate DNRA and reduce nitrate and nitrite under oxygen-
411 limited conditions. For this purpose, we incubated each strain in static (without agitation) liquid
412 culture conditions to limit oxygen availability. Overall, 68% and 77% of strains revealed a capacity

413 to reduce either nitrate (NO_3^-) or nitrite (NO_2^-), respectively, with 52% able to reduce both nitrate
414 and nitrite (Fig. 3c/d, Fig. 4 and Fig. 5). No N_2 gas production was observed, excluding
415 denitrification, which has been only rarely reported for *Streptomyces* (Albrecht et al. 1997; Shoun
416 et al. 1998; Kumon et al. 2002). The lack of N_2 generation would suggest a complete reduction of
417 nitrate/nitrite to ammonia via dissimilatory nitrate reduction. Ammonia produced by this pathway,
418 unless not incorporated by other bacteria or oxidized to other nitrogenous compounds, might
419 alkalinize the extracellular environment and thus stimulate $CaCO_3$ precipitation (Fig. 1). In order
420 to evaluate the presence of a DNRA pathway in moonmilk isolates we screened their genomes for
421 the presence of genes coding for respiratory nitrate reductases (*narGHJI*) and their associated
422 NarK-type nitrate/nitrite transporter - NarK2 (Fig. 1). While 40% of moonmilk strains encoded
423 NarK2 transporter, 30% of them possessed the respiratory nitrate reductases genes (*narGHJI*), with
424 isolates MM7, MM10, MM48, MM106, MM109, MM111, encoding a complete *nar* cluster (Table
425 1). Most of those strains were found to be among the strongest nitrate reducers under oxygen-
426 limited conditions (Fig. 4). The fact that only a minority of the moonmilk *Streptomyces* possessed
427 the genetic material to perform the first step of DNRA, while a majority (68%) was able to reduce
428 nitrate, suggests that another nitrate reduction pathway was operating under the condition tested.
429 This alternative pathway is most likely the NO_3^- and NO_2^- assimilatory process that uses nitrate
430 and nitrite as nutrient sources through assimilatory *nasA* (nitrate reductase) and *nirBD* (nitrite
431 reductase) genes, with the assistance of additional Nark-type NO_3^- transporter (Tiffert et al. 2008;
432 Amin et al. 2012; Fischer et al. 2012). Assimilatory reduction of nitrate and nitrite to ammonium
433 is highly plausible as 93% of moonmilk strains possess *nasA*, *nirBD*, and *narK* NO_3^- importer genes
434 (Table 1). When monitored on solid medium and thus without oxygen limitation, 68% and 77% of
435 the tested strains were able to reduce nitrate and nitrite, respectively (supplementary Fig. 4c/d),
436 which confirmed the high potential of moonmilk *Streptomyces* to use nitrate and nitrite as a

437 nitrogen source, as previously reported for terrestrial *Streptomyces* (Pullan et al. 2011; Fischer et
438 al. 2012). Altogether, although moonmilk *Streptomyces* possess metabolic ability to reduce nitrate
439 and nitrite, without production of gas, pointing on ammonia as a final product, we cannot at this
440 point conclude whether this process represents assimilatory or dissimilatory pathway and whether
441 DNRA is fully functional.
442

443 **Active calcium transport**

444 In addition to processes passively influencing carbonate precipitation, bacteria can also
445 actively impact this phenomenon, through an active transport of calcium ions. Banks et al. (2010)
446 suggested that the calcium-toxicity driven removal of this ion outside the bacterial cell is a factor
447 driving calcification phenotype. Therefore, we have also retrieved through an *in silico* search
448 ChaA, the $Ca^{2+}/2H^{+}$ antiporter system suggested to be involved in $CaCO_3$ deposition (Hammes and
449 Verstraete 2002; Banks et al. 2010) (Fig. 1). The presence of the *chaA* gene was confirmed for 50%
450 of moonmilk cultivable phylotypes (Table 1), extending in those strains the calcium-detoxification
451 system to their spectrum of biomineralization-related processes.
452

453 **Production of $CaCO_3$ deposits by moonmilk *Streptomyces***

454 In order to confirm whether the moonmilk cultivable *Streptomyces* could indeed produce
455 mineral deposits, we selected two phylotype representatives to be first investigated by polarized
456 light microscopy then by ESEM in low vacuum mode for the presence of calcium carbonate
457 precipitates. The selection of strains was based on their predispositions for $CaCO_3$ precipitation as
458 judged by the sum of metabolic performance observed for ureolysis and peptide/amino acid

ammonification – the two most significant activities observed for moonmilk *Streptomyces* (Fig. 4). Strains MM24 and MM99, amongst one of the best isolates based on the metabolic ranking (Fig. 4), were simultaneously cultivated on urea-containing CPA medium for two months, as well as for one month on the modified B-4 medium commonly used for $CaCO_3$ precipitation assays. Combined microscopic observations of bacterial colonies surfaces with BSE and GSE detectors revealed highly abundant calcite deposits produced by both strains in both media tested (Fig. 6 and Fig. 7). Ureolysis-mediated mineral precipitation was confirmed by the lack of any calcite in urea-deficient CPA medium for both isolates (data not shown). All the produced mineral deposits appeared bright under polarized light (data not shown). The morphology of the calcite polymorphs was comparable between the isolates, however differed between the two culture conditions. On BSE-images, bacterial colonies grown in CPA medium showed a rocky surface with discoidal- or oval-shaped structures of variable diameter that were almost completely encrusting microbial colonies (Fig. 6a/c). The mineral nature of the deposits was confirmed through their high (white) contrast on BSE-images compared to the surrounding dark organic matter of the colonies (Fig. 6a/c). In addition, their $CaCO_3$ mineral composition was confirmed by the elemental X-ray analyses (supplementary Fig. 5) and elemental mapping (Fig. 6b/d). Calcium, carbon and oxygen were present roughly in stoichiometric proportion of $CaCO_3$ in the spectra (supplementary Fig. 5), and the distribution of those elements was clearly visualized on the mapping (Fig. 6b/d). The presence of calcium was associated with $CaCO_3$ minerals, while higher proportion of carbon was associated with organic colony biomass (Fig. 6b/d). Interestingly, just on the mineral surface, dense webs of nano-sized filaments were observed (Fig. 7a-e). On high resolution BSE-images, they appeared either as dark curved filaments at the mineral surface or in the middle of mineralized wrinkles suggesting that bacteria produced minerals in which they got progressively entombed (Fig. 7a-d). The filaments free of mineral were also clearly seen interconnecting together and connecting

adjacent mineral deposits (Fig. 7e). While on the CPA medium both strains prolifically produced relatively small-sized calcite polymorphs (up to 100 µm) (Fig. 6a/c), on the B-4 medium the observed precipitates although being more scarce, were much larger (up to 400 µm) (Fig. 6e/g). The inorganic nature of the larger $CaCO_3$ deposits (Fig. 6e/g) were confirmed by X-ray elemental spectra (supplementary Fig. 5) and elemental mapping (Fig. 6f/h), which clearly distinguished $CaCO_3$ minerals from the surrounding bacterial biomass rich in carbon and oxygen. On BSE-image (Fig. 7f) and under polarized light (data not shown), tiny $CaCO_3$ deposits were also detected along randomly distributed bacterial filaments. Additionally, unlike in CPA medium where the mineral surface was rather irregular and unstructured, mineral produced by both strains in B-4 showed morphologically distinct areas, either with a smooth, radiating texture (Fig. 7h), with visible filamentous imprints (Fig. 7j) or wrinkles (Fig. 7g), that presumably corresponded to bacterial nano-sized filaments.

Potential role of cultivable moonmilk-derived *Streptomyces* in carbonate dissolution

In addition to constructive processes, bacteria are also believed to induce cave bedrock dissolution. As oppose to precipitation, a dissolution phenomenon is related to the acidification of the bacterial microenvironment, most likely as a result of organic acid production, which are the by-products of microbial carbon metabolism. The presence of detectable levels of organic acids in cave environment was previously demonstrated by *in situ* analysis via ATR-FTIR spectroscopy (Bullen et al. 2008). Released organic acids are able to bind cations such as Ca^{2+} and liberate carbonates, which can be subsequently re-precipitated to form cave secondary deposits or be used by bacteria. Therefore, we have tested the 31 phylotypes for their ability to decrease the pH of the medium through oxidative degradation of glucose based on the standardized oxidative/fermentative test (Hugh and Leifson 1953). Over 68% of isolates were found to induce

media acidification by this pathway, which was observed as yellow color to transparent halo development around the inoculum (Fig. 8a and Fig. 9). Among them, 52% of the *Streptomyces* strains exhibited either good or strong oxidative glucose respiration abilities, strongly reducing the extracellular pH (Fig. 5, Fig. 9 and supplementary Fig. 6).

We have further tested solubilization abilities related to carbon metabolism by cultivating the phylotypes in calcium carbonate containing media – either in minimal medium or in diluted nutrient agar - supplemented or not with glucose. The clear effect of glucose breakdown was observed in diluted nutrient agar in which the supplementation with the carbohydrate induced $CaCO_3$ dissolution in 26% of the isolates, while none of the phylotypes promoted dissolution in the non-supplemented medium (Fig. 8b and Fig. 9). In the non-supplemented nutrient agar, rich in organic nitrogen source, the cellular energy comes from amino acid utilization, releasing ammonia as the by-product (Fig. 1), which increases the pH of the medium and thus promotes precipitation rather than dissolution. The addition of glucose clearly induces the opposite effect but only in a minority of the isolates which suggests the preference towards amino acids as carbon source over glucose in the large majority of the studied strains (Fig. 8b and Fig. 9). On the contrary, when assays were performed in the minimal medium, $CaCO_3$ dissolution was instead rather inhibited by the exogenous supply of glucose, as only 29% of isolates showed ability to solubilize $CaCO_3$ under this condition, while in minimal media without glucose supply the dissolution phenotype was characteristic for 81% of isolates (Fig. 8c and Fig. 9). This might be probably related to the fact that in minimal medium not supplemented with glucose the only carbon source constitutes the carbonate/bicarbonate from $CaCO_3$, which is probably efficiently scavenged by cave-dwelling bacteria for autotrophic growth resulting in the high dissolution rate observed under this condition. Although *Streptomyces* are mainly heterotrophic microorganisms, autotrophic growth using CO or

529 CO_2 as a sole carbon source within members of this genus has already been reported (Kim et al.
530 1998; Gadkari et al. 1990). The identification of a high number of carbonic anhydrases together
531 with SulP transporters among moonmilk *Streptomyces* (Table 1) could propose a mechanism via
532 which extracellular bicarbonate would be incorporated into the cell and subsequently converted to
533 CO_2 (Figure 1). In the moonmilk niche that is deprived of organic carbon, the uptake of inorganic
534 carbon could thus be a possible scenario, which would primarily promote $CaCO_3$ precipitation, and
535 in a second step would lead to $CaCO_3$ dissolution, as a result of organic acids excretion. The
536 availability of glucose also induces a dissolution phenotype via release of organic acids from
537 glucose breakdown, however only in 3 out of the 31 strains tested. This indicates that, although
538 carbohydrate metabolism might somehow play a role in rock weathering, it is probably not the only
539 operating system leading to this phenomenon, particularly in carbon-limited cave environment,
540 where the source of carbon might be the rock itself.

Discussion~~Conclusions~~

If Actinobacteria really participate in the genesis of moonmilk deposits which metabolic activities would potentially be involved? This was the main question addressed in our study which used a collection of *Streptomyces* strains isolated from moonmilk in order to provide metabolic and genetic evidences of their presumed role in mediating the formation of these speleothems. Metabolic profiling revealed that all of the isolated *Streptomyces* possessed the capacity to promote calcification through at least one pathway involved in biomineralization. Ammonification of peptides/amino acids was found to be the most widespread and the strongest activity. This could be in agreement with the fact that peptides and amino acids can constitute self-sustainable sources of carbon and nitrogen for bacteria and thus support growth of microbial populations irrespectively of allochtonous nutrient input. Interestingly, genome mining extended the possible spectrum of metabolic capacities as it revealed the presence of additional pathways in each phylotype involved in biomineralization processes, either related to CO_2 hydration or active transport of calcium ions. These findings, supported by microscopy observations of bacteria-like filaments in moonmilk deposits and crystals produced by individual moonmilk-originating bacteria, confirm its biogenic origin and the importance of filamentous Actinobacteria in its genesis. However, the metabolic activities evaluated *in vitro* were not always directly related to the genetic predisposition of individual strains as some isolates with great genetic potential remained metabolically silent. This may suggest that they were grown under conditions too different from those encountered in their original niche to trigger the investigated activity or that specific environmental cues are required for their activation. Consequently, whether those processes are indeed active *in situ* also remains an open question. Additionally, our collection of moonmilk Actinobacteria, though being the most significant population from these speleothems generated so far, does not include the large majority

564 of endemic representatives which are viable but not cultivable A metaproteomic analysis of
565 proteins extracted from moonmilk deposits is most likely the only approach that would accurately
566 identify the strains that importantly participate in carbonatogenesis and the metabolic pathways
567 involved. This approach is currently under investigation.

568

569 Acknowledgments

570 MM and LM work is supported by a Research Foundation for Industry and Agriculture (FRIA)
571 grant. AN work is supported by a First Spin-off grant from the Walloon Region (Grant number:
572 1510530; FSO AntiPred). Computational resources ("durandal" grid computer) were funded by
573 three grants from the University of Liège, "Fonds spéciaux pour la recherche," "Crédit de
574 démarrage 2012" (SFRD-12/03 and SFRD-12/04) and "Crédit classique 2014" (C-14/73) and by a
575 grant from the F.R.S.-FNRS "Crédit de recherche 2014" (CDR J.0080.15). This work is supported
576 in part by the Belgian program of Interuniversity Attraction Poles initiated by the Federal Office
577 for Scientific Technical and Cultural Affairs (PAI no. P7/44). The authors thanks Isabelle Habsch
578 for microscopy sample preparation and the Centre of Aid for Research and Education in
579 Microscopy (CAREm-ULg) for giving access to SEM-equipment. SR and MH are Research
580 Associates at Belgian Fund for Scientific Research (F.R.S-FNRS).

581 Conflict of interest

582 The authors declare that they have no conflict of interest.

Figure captions

Fig. 1 Heterotrophic pathways associated with carbonatogenesis presumed to occur in *Streptomyces* species. Microbially mediated carbonate precipitation might be either linked to active transport of calcium ions across cellular membrane through $Ca^{2+}/2H^{+}$ antiporter system – ChaA, or to nitrogen cycle-related pathways – ureolysis, ammonification and dissimilatory reduction of nitrate to ammonium/ammonia (DNRA). All those pathways lead to alkalinization of the bacterial environment through the generation of ammonium, shifting the equilibrium towards carbonate/bicarbonate ions, which, upon the presence of calcium, precipitate as calcium carbonate ($CaCO_3$). ChaA, apart from providing calcium ions for potential precipitation, locally increase pH through simultaneous incorporation of protons. The urease activity seems to be linked with cytoplasmic carbonic anhydrases (β-CA), which catalyze dehydration of carbonic acid produced during ureolysis into carbon dioxide that can constitute an additional source of bicarbonate ions for precipitation. The export or import of bicarbonate ions could be potentially mediated via the sulfate transporter family protein in cluster with CA (SulP-type permease). Assimilation of organic nitrogen from amino acids releases extracellular ammonia through deamination, once the metabolic demand for nitrogen is fulfilled. The inorganic nitrogen source (NO_3^-), which is imported in *Streptomyces* by Nark-type transporters, can participate into biomineralization exclusively through dissimilatory reduction to ammonia mediated by respiratory nitrate reductases (Nar) together with potential nitrite reductases (Nir), which would be functional under dissimilatory conditions. Reduction of nitrite to ammonia in streptomycetes was found to operate through assimilatory pathway catalyzed by NasA and NirBD reductases

Fig. 2 SEM-images of nano-size filaments found in the crystal structure of moonmilk deposits from the cave "Grotte des Collemboles" (Comblain-au-Pont, Belgium). Among typical moonmilk monocrystalline rods and polycrystalline fibers indicated by white arrows **(a),** dense meshes of tiny filaments were observed, which were compacted into the stacked pellets **(b)** or dense biofilms **(c),** mostly randomly orientated, but occasionally one-way directed **(d, e).** Along **(f)** or on the tip **(g)** of some of those filaments, calcium carbonate deposition was identified**,** with some of the filaments presenting reticulated morphology **(h)** as indicated by arrows

Fig. 3 Precipitation-related metabolic activities of the moonmilk *Streptomyces*. (a) Ureolysis. **(b)** Ammonification**. (c)** Nitrate reduction. **(d)** Nitrite reduction. *Klebsiella pneumoniae* ATCC 13883 (KP), *Citrobacter freundii* ATCC 43864 (CF), *Escherichia coli* ATCC 25922 (EC) and *Pseudomonas aeruginosa* ATCC 27853 (PA) were used as positive controls for ureolysis, ammonification, nitrate and nitrite reduction tests, respectively. The observed activities are visualized for representative strains demonstrating different metabolic performance for each activity tested, designated through the symbols: (-) lack, (+/-) weak, (+) moderate, (++) good, and (+++) strong

Fig. 4 The global pattern of carbonate precipitation-associated metabolic activities of moonmilk *Streptomyces.* The heatmap plot representing metabolic performance of moonmilk *Streptomyces* strains indicated by color scale, correlated with their MLSA-based phylogenetic classification (Maciejewska et al. 2016). The total value represents the sum of metabolic performance observed for ureolysis and amino acids ammonification, ranking the isolates according to their metabolic predispositions for calcium carbonate precipitation for the tested activities. The metabolic performance of nitrate/nitrite reduction test was not included into the final

628 ranking. Abbreviations: U, ureolysis; A, peptide/amino acid ammonification; T, total sum of
629 activities for ureolysis and amino acid ammonification; NO_3^-, nitrate reduction; NO_2^-, nitrite
630 reduction

631

632 **Fig. 5 Percentage of moonmilk *Streptomyces* displaying carbonatogenesis related activities *in***
633 ***vitro* within different metabolic categories.** (-) lack, (+/-) weak, (+) moderate, (++) good, and
634 (+++) strong

635

636 **Fig. 6 Low vacuum-SEM-BSE images** (a, c, e, g) **and X-ray elemental mappings** (b, d, f, h) **of**
637 **$CaCO_3$ deposits produced by MM24** (a-b, e-f) **and MM99** (c-d, g-h) **isolates.** Abundant mineral
638 deposits produced by isolates MM99 **(a)** and MM24 **(c)** in CPA medium, nearly encrusting the
639 whole microbial colony, were morphologically different from less abundant, but much bigger,
640 mineral polymorphs produced in modified B-4 agar by MM99 **(e)** and MM24 **(g).** The observed
641 precipitates were found to be $CaCO_3$ minerals as revealed by elemental spectra (supplementary Fig.
642 5) and mappings in both media and for both isolates (MM99 **(b)** and MM24 **(d)** in CPA, MM99 **(f)**
643 and MM24 **(h)** in modified B-4). The mappings for MM99 and MM24 in B-4 are marked with the
644 white squares. The mappings are combined images in which detected dominant elements, namely
645 carbon (C), oxygen (O), and calcium (Ca) are assigned to a defined color

646

647 **Fig. 7 Biogenic signatures within mineral deposits produced by moonmilk-originating**
648 ***Streptomyces* (LV-SEM-BSE images).** Along with the different morphologies of produced
649 mineral deposits specific to the culture conditions used, numerous bacterial imprints were
650 observed. *Streptomyces* filaments were completely incorporated into the produced minerals as
651 observed for MM99 **(a/b),** MM24 **(c/d/e)** in CPA medium, as well as for MM99 **(g)** and MM24

652 **(i/j)** in modified B-4 agar. Their mineralization also appeared as wrinkles each containing a
653 bacterial filament suggesting their progressive encrustation within the mineral **(b/e/g,** arrows**).**
654 Alternatively, non-mineralized microbial filaments were seen interconnecting adjacent mineral
655 deposits, as detected for MM24 in CPA **(c/e,** arrows**)**, or possible compacted aggregates of
656 filaments were observed at the edges of the mineral produced by MM99 in B-4 **(h).** Initial steps of
657 mineral deposition were detected along bacterial filaments in modified B-4 culture of isolate
658 MM99 **(f,** arrows**)**
659
660 **Fig. 8 Dissolution-related metabolic activities of the moonmilk *Streptomyces*.** Metabolic
661 performance observed for oxidative glucose degradation **(a)**, and calcium carbonate dissolution in
662 diluted nutrient agar **(b)** or minimal media **(c).** *Pseudomonas aeruginosa* ATCC 27853 (PA) was
663 used as positive control in glucose oxidative assay. The metabolic performance is designated
664 through the symbols: (-) lack, (+/-) weak, (+) moderate, (++) good, and (+++) strong activity.
665 Media not supplemented with glucose are in the upper line in panel **b** and **c**, while media with
666 addition of glucose are displayed in the bottom line of the corresponding panels
667
668 **Fig. 9 The global pattern of carbonate dissolution-associated metabolic activities of moonmilk**
669 ***Streptomyces.*** The heatmap plot representing metabolic performance of moonmilk *Streptomyces*
670 strains indicated by color scale, correlated with their MLSA-based phylogenetic classification
671 (Maciejewska et al. 2016). Abbreviations: O, glucose oxidation; MM, minimal media with $CaCO_3$;
672 MMg, minimal media with $CaCO_3$ and glucose; NA, diluted nutrient agar with $CaCO_3$; NAg,
673 diluted nutrient agar with $CaCO_3$ and glucose

674 # Tables

675 **Table 1.** *In silico* prediction of individual genes putatively involved in the moonmilk
676 biomineralization process retrieved from moonmilk-originating *Streptomyces* strains, including
677 genes related to ureolysis (*ure*), nitrate/nitrite transport (*narK*) and reduction (*nar*/*nas*/*nir*), carbon
678 dioxide (CO_2) hydration (carbonic anhydrase - CA), and active transport of calcium ions through
679 $Ca^{2+}/2H^{+}$ antiporter system (*chaA*).

	Ureolysis							NO_3^- / NO_2^- transport		Respiratory NO_3^- reduction					Assimilatory NO_3^- reduction	NO_2^- reduction			CO_2 hydration			Ca^{2+} transport
strain	*ureA*	*ureB*	*ureAB*	*ureC*	*ureF*	*ureG*	*ureD*	*narK2*	*narK*	*narG*	*narH*	*narJ*	*narJ2*	*narI*	*nasA*	*nirB1*	*nirB2*	*nirD*	β-CA (1)	β-CA (2)	*sulP*	*chaA*
MM1	1	1	2	3	1	1	2	-	+	-	-	-	-	-	1	1	1	1	2	1	1	-
MM3	1	1	2	3	2	2	3	-	+	-	-	-	-	-	1	1	1	1	2	1	1	-
MM5	1	1	2	3	2	2	2	-	+	-	-	-	-	-	1	1	1	1	3	3	1	1
MM6	1	1	1	3	1	1	1	-	+	-	-	-	-	-	1	1	2	2	4	-	1	1
MM7	2	2	2	3	2	2	2	+	+	1	1	-	1	1	1	1	1	1	1	1	1	-
MM10	1	1	1	2	2	2	2	+	+	3	2	1	1	2	1	1	1	1	2	1	1	-
MM12	1	1	2	3	3	3	3	-	+	-	-	-	-	-	1	1	1	1	2	2	-	1
MM13	1	1	1	2	2	2	2	+	+	1	-	-	-	1	1	1	1	1	2	1	1	1
MM14	1	1	2	3	2	2	2	-	+	-	1	-	1	1	1	1	1	1	1	2	1	-
MM17	1	1	3	3	2	2	2	-	+	1	-	-	-	-	1	1	1	1	6	1	1	1
MM19	1	1	1	2	1	1	1	-	+	-	-	-	-	-	1	1	1	1	1	1	1	-
MM21	1	1	2	3	2	2	2	-	+	-	-	-	-	-	1	1	1	1	2	1	1	-
MM23	1	1	2	3	2	2	2	-	+	-	-	-	-	-	1	1	1	1	1	1	1	-
MM24	2	2	2	5	2	2	4	+	+	-	-	-	-	-	1	1	1	1	2	2	1	1
MM44	1	1	2	3	2	2	2	-	+	-	-	-	-	-	1	1	1	1	2	1	1	-
MM48	2	2	2	4	2	2	2	-	+	1	1	-	1	1	2	1	2	1	5	1	1	1
MM59	1	1	-	1	1	1	1	-	+	-	-	-	-	-	1	1	1	1	3	2	1	1
MM68	1	1	1	2	3	2	2	-	+	-	-	-	-	-	1	1	1	1	2	2	1	1*
MM99	3	3	1	4	3	3	3	+	-	-	-	-	-	-	1	-	-	-	1	1	1	-
MM100	1	1	2	4	2	2	2	+	+	-	-	-	-	-	2	1	1	1	2	1	-	-
MM104	1	1	1	1	1	1	1	-	+	-	-	-	-	-	-	1	1	1	2	3	1	1
MM105	1	1	3	4	1	1	1	+	+	-	-	-	-	-	1	1	1	1	1	-	1	-
MM106	2	2	-	2	2	2	2	+	+	2	2	-	2	2	1	1	1	1	1	-	1	1
MM107	-	-	-	1	-	-	-	-	-	-	-	-	-	-	-	-	-	-	3	2	1	1
MM108	1	1	3	4	1	1	1	+	+	-	-	-	-	-	2	1	1	1	3	1	1	1
MM109	1	1	2	3	2	2	2	+	+	2	1	-	1	2	1	1	1	1	2	-	1	-
MM111	2	2	2	4	2	2	2	-	+	1	1	-	1	1	1	1	1	1	1	1	1	1
MM117	1	1	1	2	1	1	1	+	+	-	-	-	-	-	2	1	1	1	1	1	1	-
MM122	2	2	2	4	3	3	3	+	+	-	-	-	-	-	1	1	1	1	1	3	-	-
MM128	1	1	1	2	1	1	1	-	+	-	-	-	-	-	1	1	1	1	2	2	1	1

Abbreviations: CA_sulf, sulfate transporter family protein in cluster with carbonic anhydrase; * pseudogene

References

Achal V, Pan X (2011) Characterization of urease and carbonic anhydrase producing bacteria and their role in calcite precipitation. Curr Microbiol 62:894–902. doi: 10.1007/s00284-010-9801-4

Albrecht A, Ottow JCG, Benckiser G, et al (1997) Incomplete denitrification (NO and N_2O) from nitrate by *Streptomyces violaceoruber* and *S. nitrosporeus* revealed by acetylene inhibition and 15N gas chromatography-quadrupole mass spectrometry analyses. Naturwissenschaften 84:145–147.

Amin R, Reuther J, Bera A, et al (2012) A novel GlnR target gene, *nnaR*, is involved in nitrate/nitrite assimilation in Streptomyces coelicolor. Microbiology 158:1172–1182. doi: 10.1099/mic.0.054817-0

Axenov-Gibanov D V., Voytsekhovskaya I V., Tokovenko BT, et al (2016) Actinobacteria isolated from an underground lake and moonmilk speleothem from the biggest conglomeratic karstic cave in Siberia as sources of novel biologically active compounds. PLoS One 11(2). doi: 10.1371/journal.pone.0149216

Banks ED, Taylor NM, Gulley J, et al (2010) Bacterial Calcium Carbonate Precipitation in Cave Environments: A Function of Calcium Homeostasis. Geomicrobiol J 27:444–454. doi: 10.1080/01490450903485136

Barton HA, Northup DE (2007) Geomicrobiology in cave environments: Past, current and future perspectives. J Cave Karst Stud 69:163–178.

Baskar S, Baskar R, Routh J (2011) Biogenic Evidences of Moonmilk Deposition in the Mawmluh Cave, Meghalaya, India. Geomicrobiol J 28:252–265. doi: 10.1080/01490451.2010.494096Bentley SD, Chater KF, Cerdeño-Tárraga a-M, et al (2002)

704 Complete genome sequence of the model actinomycete *Streptomyces coelicolor* A3(2).
705 Nature 417:141–147. doi: 10.1038/417141a
706 Bindschedler S, Cailleau G, Braissant O, et al (2014) Unravelling the enigmatic origin of calcitic
707 nanofibres in soils and caves: purely physicochemical or biogenic processes? Biogeosciences
708 2809–2825.
709 Bindschedler S, Milliere L, Cailleau G, et al (2010) Calcitic nanofibres in soils and caves: a putative
710 fungal contribution to carbonatogenesis. Geol Soc London, Spec Publ 336:225–238. doi:
711 10.1144/SP336.11
712 Borodina I, Krabben P, Nielsen J (2005) Genome-scale analysis of *Streptomyces coelicolor* A3(2)
713 metabolism. Genome Res 15:820–829. doi: 10.1101/gr.3364705
714 Borsato A, Frisia S, Jones B, van der Borg K (2000) Calcite moonmilk: crystal morphology and
715 environment of formation in caves in the italian Alps. J Sediment Res 70:1179–1190. doi:
716 10.1306/032300701171
717 Braissant O, Bindschedler S, Daniels A, et al (2012) Microbiological activities in moonmilk
718 monitored using isothermal microcalorimetry (Cave of Vers Chez Le Brandt, Neuchatel,
719 Switzerland). J Cave Karst Stud 74:116–126.
720 Bullen H, Oehrle S, Bennett A, et al (2008) Use of Attenuated Total Reflectance Fourier Transform
721 Infrared Spectroscopy To Identify Microbial Metabolic Products on Carbonate Mineral
722 Surfaces. Appl Environ Microbiol 74:4553–4559.
723 Cacchio P, Ferrini G, Ercole C, Lepidi A (2014) Biogenicity and Characterization of Moonmilk in
724 the Grotta Nera (Majella National Park, Abruzzi, Central Italy). J Cave Karst Stud 76:88–103.
725 Cailleau G, Verrecchia EP, Braissant O, Emmanuel L (2009) The biogenic origin of needle fibre
726 calcite. Sedimentology 56:1858–1875. doi: 10.1111/j.1365-3091.2009.01060.x
727 Cañaveras JC, Cuezva S, Sanchez-Moral S, et al (2006) On the origin of fiber calcite crystals in

728 moonmilk deposits. Naturwissenschaften 93:27–32. doi: 10.1007/s00114-005-0052-3

729 Cañaveras JC, Hoyos Gómez M, Sánchez-Moral S, et al (1999) Microbial Communities Associated
730 With Hydromagnesite and Needle-Fiber Aragonite Deposits in a Karstic Cave (Altamira,
731 Northern Spain). Geomicrobiol J 16:9–25. doi: 10.1080/014904599270712

732 Castanier S, M G Le, Perthuisot J, Le Metayer-Levrel G (2000) Bacterial roles in the precipitation
733 of carbonate minerals. In: Microbial sediments. pp 32–39.

734 Cuezva S, Fernandez-Cortes A, Porca E, et al (2012) The biogeochemical role of Actinobacteria
735 in Altamira Cave, Spain. FEMS Microbiol Ecol 81:281–290. doi: 10.1111/j.1574-
736 6941.2012.01391.x

737 Deutch CE, Perera GS (1992) Myceloid cell formation in *Arthrobacter globiformis* during osmotic
738 stress. Journal of Applied Bacteriology, 72:493–499. doi:10.1111/j.1365-
739 2672.1992.tb01865.x

740 Dhami NK, Reddy MS, Mukherjee A (2014) Synergistic role of bacterial urease and carbonic
741 anhydrase in carbonate mineralization. Appl Biochem Biotechnol 172:2552–2561. doi:
742 10.1007/s12010-013-0694-0

743 Eddy S (1998) Profile hidden Markov models. Bioinformatics 14:755–763. doi: btb114 [pii]

744 Engel AS, Paoletti MG, Beggio M, et al (2013) Comparative microbial community composition
745 from secondary carbonate (moonmilk) deposits: implications for the *Cansiliella servadeii*
746 cave hygropetric food web. Int J Speleol 42:181–192.

747 Felce J, Saier MH (2005) Carbonic anhydrases fused to anion transporters of the SulP family:
748 Evidence for a novel type of bicarbonate transporter. J Mol Microbiol Biotechnol 8:169–176.
749 doi: 10.1159/000085789

750 Fischer M, Alderson J, Van Keulen G, et al (2010) The obligate aerobe *Streptomyces coelicolor*
751 A3(2) synthesizes three active respiratory nitrate reductases. Microbiology 156:3166–3179.

752 doi: 10.1099/mic.0.042572-0

753 Fischer M, Falke D, Pawlik T, Sawers RG (2014) Oxygen-dependent control of respiratory nitrate
754 reduction in mycelium of *Streptomyces coelicolor* A3(2). J Bacteriol 196:4152–4162. doi:
755 10.1128/JB.02202-14

756 Fischer M, Schmidt C, Falke D, Sawers RG (2012) Terminal reduction reactions of nitrate and
757 sulfate assimilation in *Streptomyces coelicolor* A3(2): identification of genes encoding nitrite
758 and sulfite reductases. Res Microbiol 165:340–348.

759 Folk RL (1993) SEM Imaging of Bacteria and Nannobacteria in Carbonate Sediments and Rocks.
760 Journal of Sedimentary Petrology 63:990–999.

761 Folk RL, Chafetz HS (2000) Bacterially Induced Microscale and Nanoscale Carbonate Precipitates.
762 In: Microbial Sediments. Springer Berlin Heidelberg, pp 40–49.

763 Food and Agriculture Organization of the United Nations (1983) A programme of investigations
764 on the hydrobiology of fish ponds (Microbiological investigations).

765 Gadkari D, Schricker K, Acker G, et al (1990) *Streptomyces thermoautotrophicus* sp. nov., a
766 Thermophilic CO- and H2-Oxidizing Obligate Chemolithoautotroph. Appl Environ Microbiol
767 56:3727–3734.

768 Ghai R, Mizuno CM, Picazo A, et al (2013) Metagenomics uncovers a new group of low GC and
769 ultra-small marine Actinobacteria. Sci. Rep 3:2471. doi:10.1038/srep02471

770 Hahn MW (2004) Broad diversity of viable bacteria in 'sterile' (0.2 μm) filtered water. Research
771 in Microbiology 155:688–691.

772 Hammad I, Talkhan F, Zoheir A (2013) Urease activity and induction of calcium carbonate
773 precipitation by *Sporosarcina pasteurii* NCIMB 8841. J Appl Sci Resear 9:1525–1533.

774 Hammes F, Verstraete W (2002) Key roles of pH and calcium metabolism in microbial carbonate
775 precipitation. Rev Environ Sci Biotechnol 1:3–7. doi: 10.1023/A:1015135629155

776 Harmon RS, Atkinson T., Atkinson J. (1983) The Mineralogy of Castleguard Cave, Columbia
777 Icefields, Alberta, Canada. Arct Alp Res 15:503–516.
778 Hugh R, Leifson E (1953) The taxonomic significance of fermentative versus oxidative metabolism
779 of carbohydrates by various gram negative bacteria. J Bacteriol 66:24–26.
780 Hyatt D, Chen G-L, Locascio PF, et al (2010) Prodigal: prokaryotic gene recognition and
781 translation initiation site identification. BMC Bioinformatics 11:119. doi: 10.1186/1471-
782 2105-11-119
783 Jones B (2010) Microbes in caves: agents of calcite corrosion and precipitation. Geol Soc London,
784 Spec Publ 336:7–30. doi: 10.1144/SP336.2
785 Jones DS, Albrecht HL, Dawson KS, et al (2011) Community genomic analysis of an extremely
786 acidophilic sulfur-oxidizing biofilm. ISME J 6:158–170. doi: 10.1038/ismej.2011.75
787 Kieser T, Bibb MJ, Buttner MJ, et al (2000) Practical *Streptomyces* Genetics. John Innes Cent. Ltd.
788 529.
789 Kim SB, Falconer C, Williams E, Goodfellow M (1998) *Streptomyces thermocarboxydovorans* sp.
790 nov. and *Streptomyces thermocarboxydus* sp. nov., two moderately thermophilic
791 carboxydotrophic species from soil. Int J Syst Evol Microbiol 48:59–68.
792 Kumon Y, Sasaki Y, Kato I, et al (2002) Codenitrification and denitrification are dual metabolic
793 pathways through which dinitrogen evolves from nitrate in *Streptomyces antibioticus*. J
794 Bacteriol 184:2963–2968. doi: 10.1128/JB.184.11.2963-2968.2002
795 Lechner M, Findeiß S, Steiner L, et al (2010) Proteinortho: Detection of (Co-)orthologs in large-
796 scale analysis. BMC Bioinformatics 21:124. doi**:** 10.1186/1471-2105-12-124
797 Li Q, Chen X, Jiang Y, Jiang C (2016) Cultural, Physiological, and Biochemical Identification of
798 Actinobacteria. In: Actinobacteria - Basics and Biotechnological Applications. doi:
799 10.5772/61462

800 Maciejewska M, Adam D, Martinet L, et al (2016) A Phenotypic and Genotypic Analysis of the
801 Antimicrobial Potential of Cultivable *Streptomyces* isolated from Cave Moonmilk Deposits.
802 Front Microbiol. doi: 10.3389/fmicb.2016.01455
803 Maniloff J (1997) Nannobacteria: size limits and evidence. Nature 276:1776.
804 Melim L, Northup DE, Spilde M, Boston PJ (2015) Update: Living Reticulated Filaments from
805 Herbstlabyrinth-Adventhöhle Cave System, Germany. J Caves Karst Stud: the National
806 Speleological Society bulletin 77(2):87-90. doi: 10.4311/2015MB0112
807 Melim LA, Northup DE, Spilde MN, et al (2008) Reticulated filaments in cave pool speleothems:
808 Microbe or mineral? J Cave Karst Stud 70:135–141.
809 Melim LA, Shinglman KM, Boston PJ, et al (2001) Evidence for Microbial Involvement in Pool
810 Finger Precipitation, Hidden Cave, New Mexico. Geomicrobiol J 18:311–329. doi:
811 10.1080/01490450152467813
812 Mendoza MLZ, Lundberg J, Ivarsson M, et al (2016) Metagenomic analysis from the interior of a
813 speleothem in Tjuv-Ante's cave, Northern Sweden. PLoS One 11(3). doi:
814 10.1371/journal.pone.0151577
815 Miller AZ, Hernández-Mariné M, Jurado V, et al (2012) Enigmatic reticulated filaments in
816 subsurface granite. Environ Microbiol Rep 4:596–603. doi: 10.1111/j.1758-
817 2229.2012.00375.x
818 Northup DE, Barns SM, Yu LE, et al (2003) Diverse microbial communities inhabiting
819 ferromanganese deposits in Lechuguilla and Spider Caves. Environ Microbiol 5:1071–1086.
820 doi: 10.1046/j.1462-2920.2003.00500.x
821 Northup DE, Lavoie KH (2001) Geomicrobiology of Caves: A Review. Geomicrobiol J 18:199–
822 222. doi: 10.1080/01490450152467750
823 Northup DE, Melim L a., Spilde MN, et al (2011) Lava Cave Microbial Communities Within Mats

824 and Secondary Mineral Deposits: Implications for Life Detection on Other Planets.
825 Astrobiology 11:601–618. doi: 10.1089/ast.2010.0562
826 Pine L, Boone CJ (1967) Comparative Cell Wall Analyses of Morphological Forms Within the
827 Genus *Actinomyces*. J Bacteriol 94:875–883.
828 Portillo MC, Gonzalez JM (2011) Moonmilk Deposits Originate from Specific Bacterial
829 Communities in Altamira Cave (Spain). Microb Ecol 61:182–189. doi: 10.1007/s00248-010-
830 9731-5
831 Portillo MC, Leff JW, Lauber CL, Fierer N (2013) Cell Size Distributions of Soil Bacterial and
832 Archaeal Taxa. Appl Environ Microbiol 79:7610–7617. doi: 10.1128/AEM.02710-13
833 Portillo MC, Porca E, Cuezva S, et al (2009) Is the availability of different nutrients a critical factor
834 for the impact of bacteria on subterraneous carbon budgets? Naturwissenschaften 96:1035–
835 1042. doi: 10.1007/s00114-009-0562-5
836 Prakash SB, Debnath M, Prasad GB (2012) Microbes: Concepts and Applications. Wiley-
837 Blackwell, pp 491–493, doi: 10.1002/9781118311912.
838 Price GD, Woodger FJ, Badger MR, et al (2004) Identification of a *SulP*-type bicarbonate
839 transporter in marine cyanobacteria. Proc Natl Acad Sci U S A 101:18228–18233. doi:
840 10.1073/pnas.0405211101
841 Pullan ST, Chandra G, Bibb MJ, Merrick M (2011) Genome-wide analysis of the role of GlnR in
842 *Streptomyces venezuelae* provides new insights into global nitrogen regulation in
843 actinomycetes. BMC Genomics 12:175. doi: 10.1186/1471-2164-12-175
844 Reitschuler C, Lins P, Schwarzenauer T, et al (2015) New Undescribed Lineages of Non-
845 extremophilic Archaea Form a Homogeneous and Dominant Element Within Alpine
846 Moonmilk Microbiomes. Geomicrobiol J 32: 890-902.
847 doi.org/10.1080/01490451.2015.1025317

848 Reitschuler C, Lins P, Wagner AO, Illmer P (2014) Cultivation of moonmilk-born non-
849 extremophilic Thaumand Euryarchaeota in mixed culture. Anaerobe 29:73–79. doi:
850 10.1016/j.anaerobe.2013.10.002
851 Reitschuler C, Spötl C, Hofmann K, et al (2016) Archaeal Distribution in Moonmilk Deposits from
852 Alpine Caves and Their Ecophysiological Potential. Microb Ecol 71:686–699.
853 Richter DK, Immenhauser A, Neuser RD (2008) Electron backscatter diffraction documents
854 randomly orientated c-axes in moonmilk calcite fibres: Evidence for biologically induced
855 precipitation. Sedimentology 55:487–497. doi: 10.1111/j.1365-3091.2007.00915.x
856 Rooney DC, Hutchens E, Clipson N, et al (2010) Microbial Community Diversity of Moonmilk
857 Deposits at Ballynamintra Cave, Co. Waterford, Ireland. Microb Ecol 60:753–761. doi:
858 10.1007/s00248-010-9693-7
859 Sanchez-Moral S, Portillo MC, Janices I, et al (2012) The role of microorganisms in the formation
860 of calcitic moonmilk deposits and speleothems in Altamira Cave. Geomorphology 139–
861 140:285–292. doi: 10.1016/j.geomorph.2011.10.030
862 Shoun H, Kano M, Baba I, et al (1998) Denitrification by actinomycetes and purification of
863 dissimilatory nitrite reductase and azurin from *Streptomyces thioluteus*. J Bacteriol 180:4413–
864 4415.
865 Smith KS, Ferry JG (2000) Prokaryotic carbonic anhydrases. FEMS Microbiol. Rev. 24:335–366.
866 Spilde MN, Northup DE, Boston PJ, et al (2005) Geomicrobiology of Cave Ferromanganese
867 Deposits: A Field and Laboratory Investigation. Geomicrobiol J 22:99–116. doi:
868 10.1080/01490450590945889
869 Steinberger RE, Allen AR, Hansma HG, Holden PA (2002) Elongation Correlates with Nutrient
870 Deprivation in *Pseudomonas aeruginosa* Unsaturated Biofilms. Microb Ecol 43:416–423.
871 doi: 10.1007/s00248-001-1063-z

872 Stocks-Fischer S, Galinat JK, Bang SS (1999) Microbiological precipitation of $CaCO_3$. Soil Biol
873 Biochem 31:1563–1571. doi: 10.1016/S0038-0717(99)00082-6
874 Tiffert Y, Supra P, Wurm R, et al (2008) The *Streptomyces coelicolor* GlnR regulon: Identification
875 of new GlnR targets and evidence for a central role of GlnR in nitrogen metabolism in
876 actinomycetes. Mol Microbiol 67:861–880. doi: 10.1111/j.1365-2958.2007.06092.x
877 Tisato N, Torriani SFF, Monteux S, et al (2015) Microbial mediation of complex subterranean
878 mineral structures. Sci Rep 5:15525. doi: 10.1038/srep15525
879 Uwins PJR, Taylor AP, Webb RI (2000) Nannobacteria, fiction or fact? In: Organic Matter and
880 Mineralisation: Thermal Alteration, Hydrocarbon Generation and Role in Metallogenesis. pp
881 421–444
882 Verrecchia EP, Verrecchia KE (1994) Needle-fiber calcite: a critical review and a proposed
883 classification. J Sediment Res 64. doi: 10.1306/D4267E33-2B26-11D7-8648000102C1865D
884 Wills AP, Chan ECS (1978) Morphogenetic expression of *Arthrobacter globiformis* 425 in
885 continuous culture with carbon or biotin limitation. Can J Microbiol 24:28–30. doi:
886 10.1139/m78-005
887 Young KD (2006) The Selective Value of Bacterial Shape. Microbiol Mol Biol Rev 70:660–703.
888 doi: 10.1128/MMBR.00001-06

889
890
891

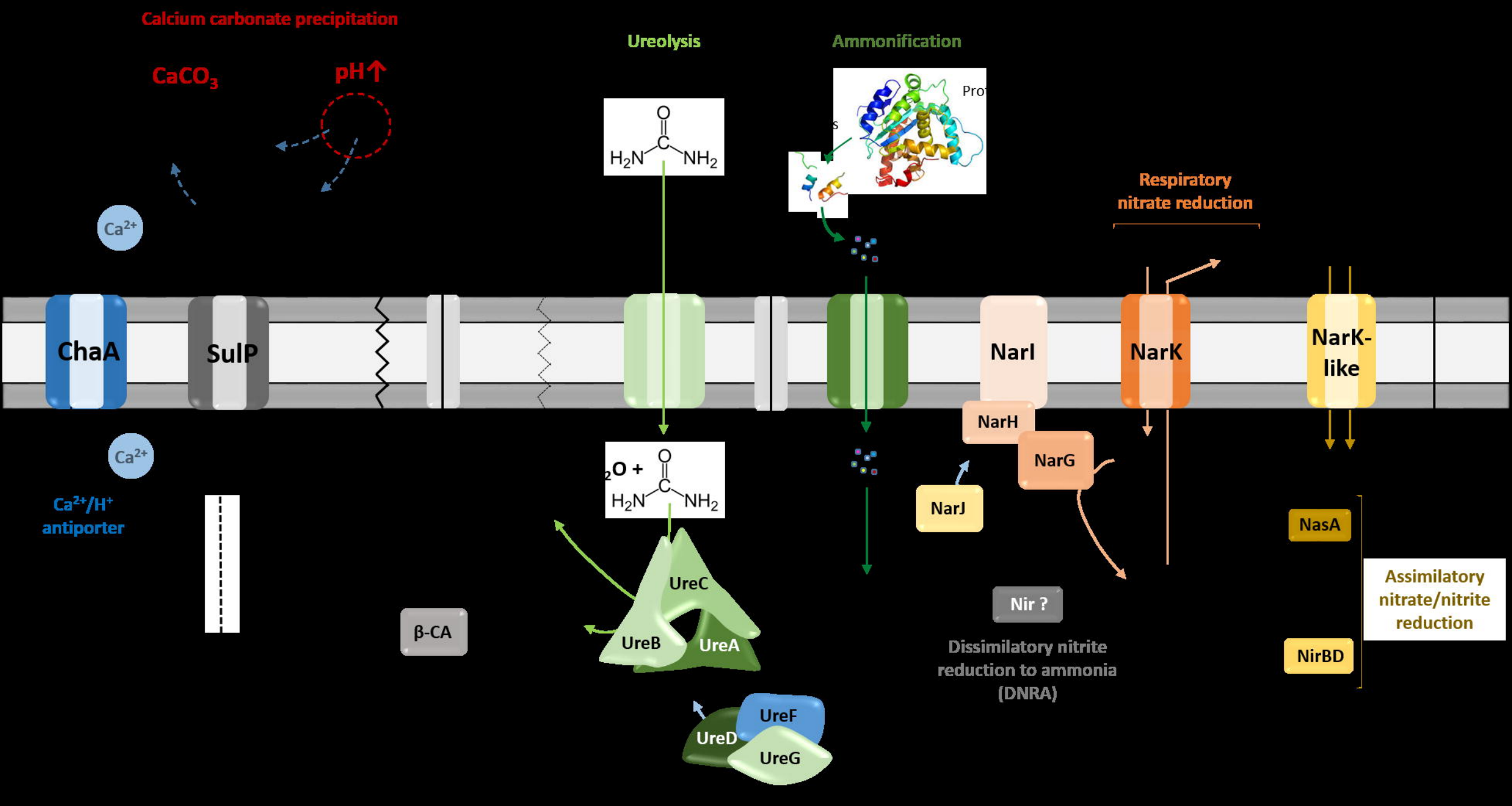
Calcium carbonate precipitation
$CaCO_3$
pH↑
Ureolysis
Ammonification
Respiratory nitrate reduction
Ca^{2+}
ChaA
SulP
NarI
NarK
NarK-like
NarH
NarG
NarJ
Ca^{2+}
Ca^{2+}/H^+ antiporter
β-CA
UreC
UreB
UreA
UreF
UreD
UreG
Nir ?
Dissimilatory nitrite reduction to ammonia (DNRA)
NasA
NirBD
Assimilatory nitrate/nitrite reduction

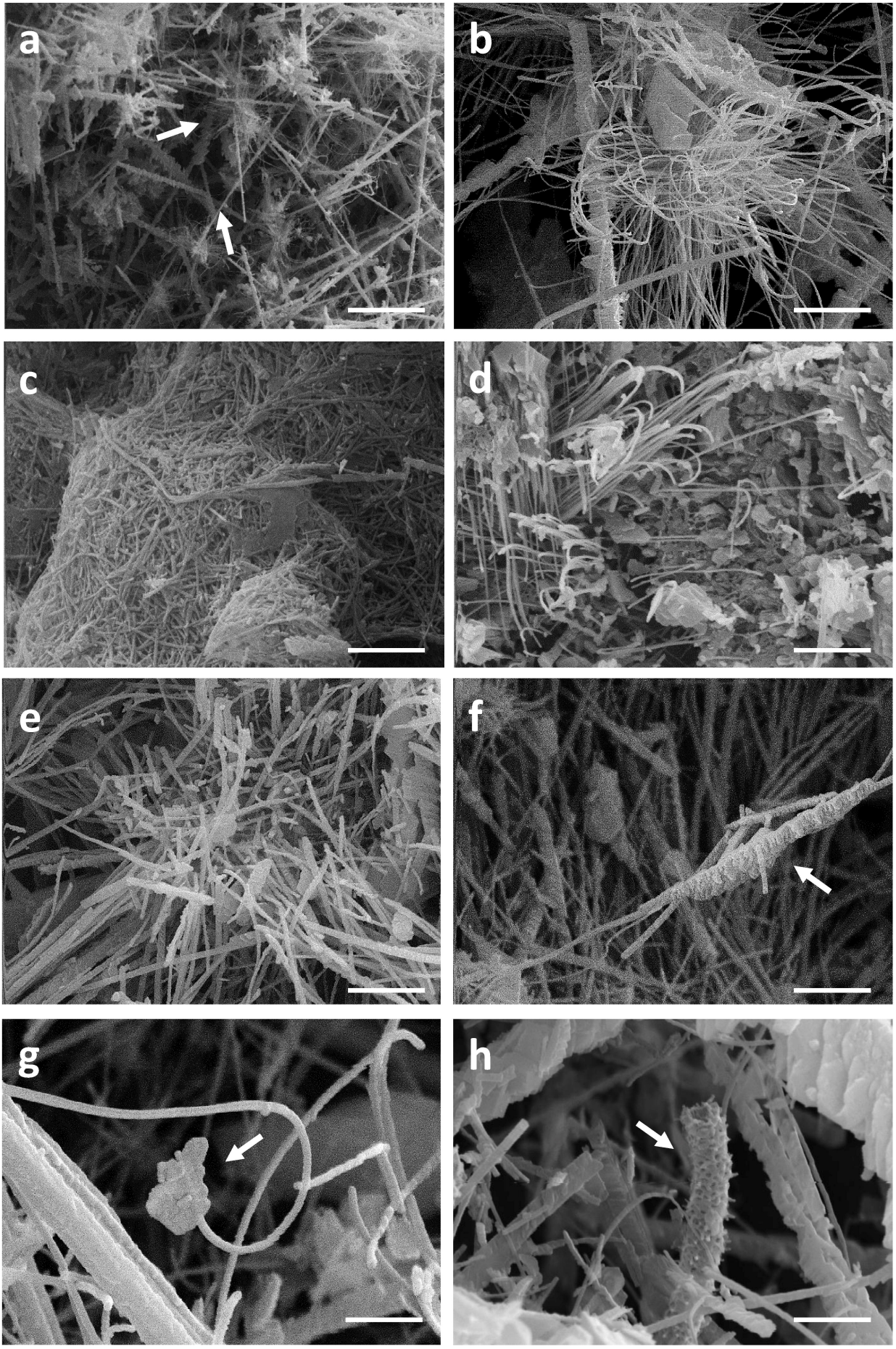
a
b
c
d
e
f
g
h

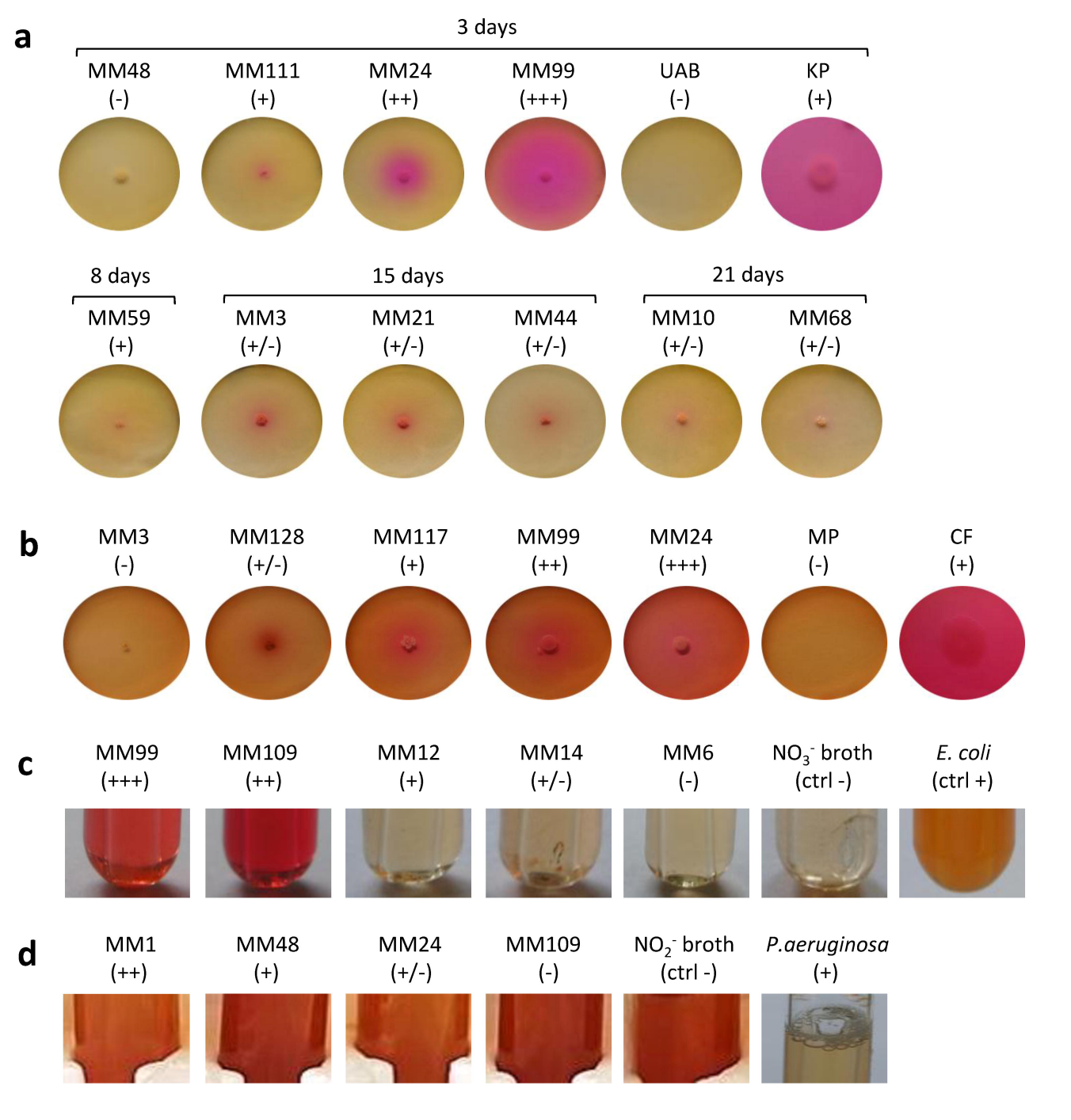
a
3 days
MM48
(-)
MM111
(+)
MM24
(++)
MM99
(+++)
UAB
(-)
KP
(+)
8 days
15 days
21 days
MM59
(+)
MM3
(+/-)
MM21
(+/-)
MM44
(+/-)
MM10
(+/-)
MM68
(+/-)
b
MM3
(-)
MM128
(+/-)
MM117
(+)
MM99
(++)
MM24
(+++)
MP
(-)
CF
(+)
c
MM99
(+++)
MM109
(++)
MM12
(+)
MM14
(+/-)
MM6
(-)
NO3- broth
(ctrl -)
E. coli
(ctrl +)
d
MM1
(++)
MM48
(+)
MM24
(+/-)
MM109
(-)
NO2- broth
(ctrl -)
P.aeruginosa
(+)

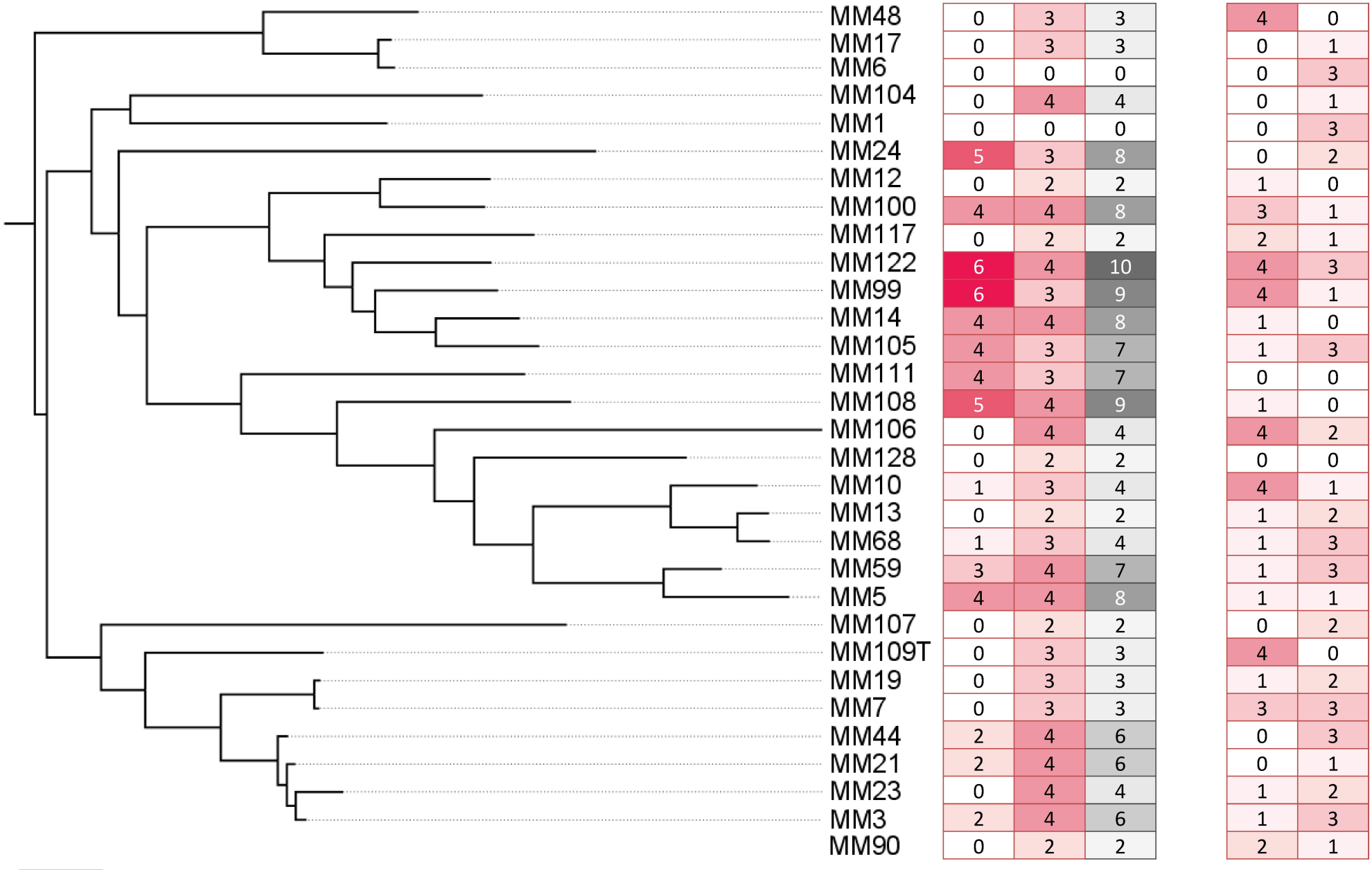
U
A
Total
NO_3^-
NO_2^-
MM48 0 3 3 4 0
MM17 0 3 3 0 1
MM6 0 0 0 0 3
MM104 0 4 4 0 1
MM1 0 0 0 0 3
MM24 5 3 8 0 2
MM12 0 2 2 1 0
MM100 4 4 8 3 1
MM117 0 2 2 2 1
MM122 6 4 10 4 3
MM99 6 3 9 4 1
MM14 4 4 8 1 0
MM105 4 3 7 1 3
MM111 4 3 7 0 0
MM108 5 4 9 1 0
MM106 0 4 4 4 2
MM128 0 2 2 0 0
MM10 1 3 4 4 1
MM13 0 2 2 1 2
MM68 1 3 4 1 3
MM59 3 4 7 1 3
MM5 4 4 8 1 1
MM107 0 2 2 0 2
MM109T 0 3 3 4 0
MM19 0 3 3 1 2
MM7 0 3 3 3 3
MM44 2 4 6 0 3
MM21 2 4 6 0 1
MM23 0 4 4 1 2
MM3 2 4 6 1 3
MM90 0 2 2 2 1
0.04

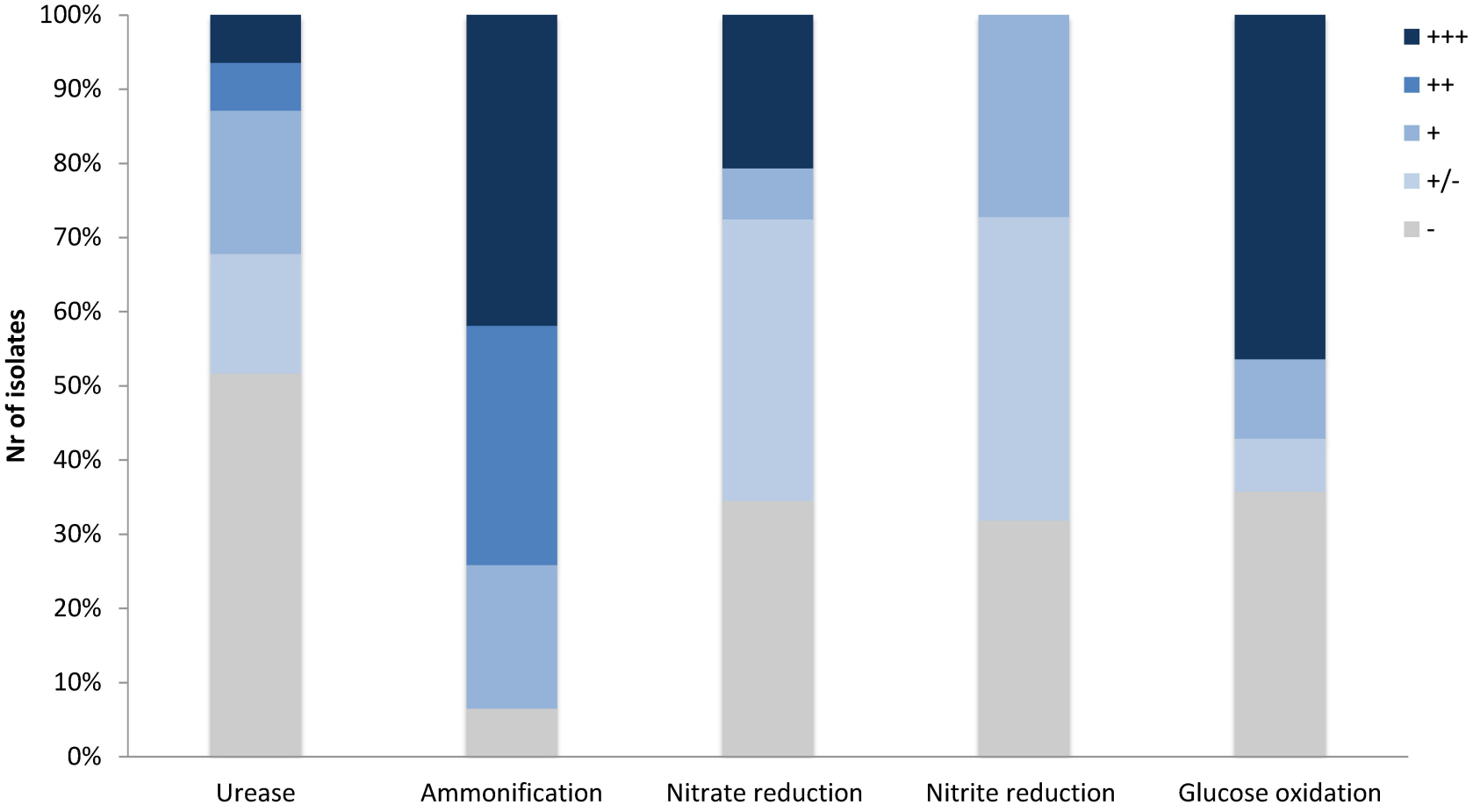
100%
90%
80%
70%
60%
50%
40%
30%
20%
10%
0%
Nr of isolates
+++
++
+
+/-
-
Urease
Ammonification
Nitrate reduction
Nitrite reduction
Glucose oxidation

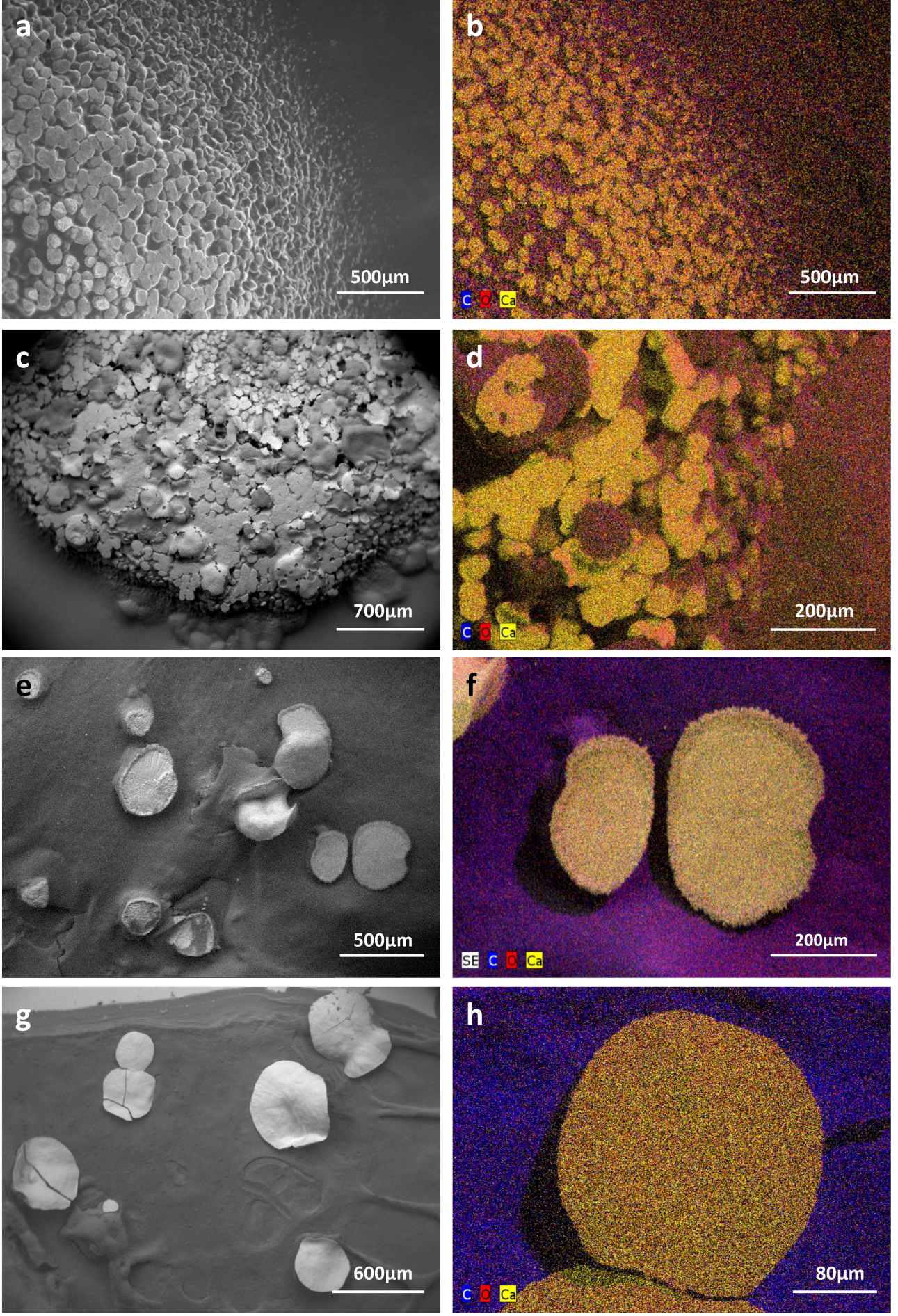
a
500µm
b
C O Ca
500µm
c
700µm
d
C O Ca
200µm
e
500µm
f
SE C O Ca
200µm
g
600µm
h
C O Ca
80µm

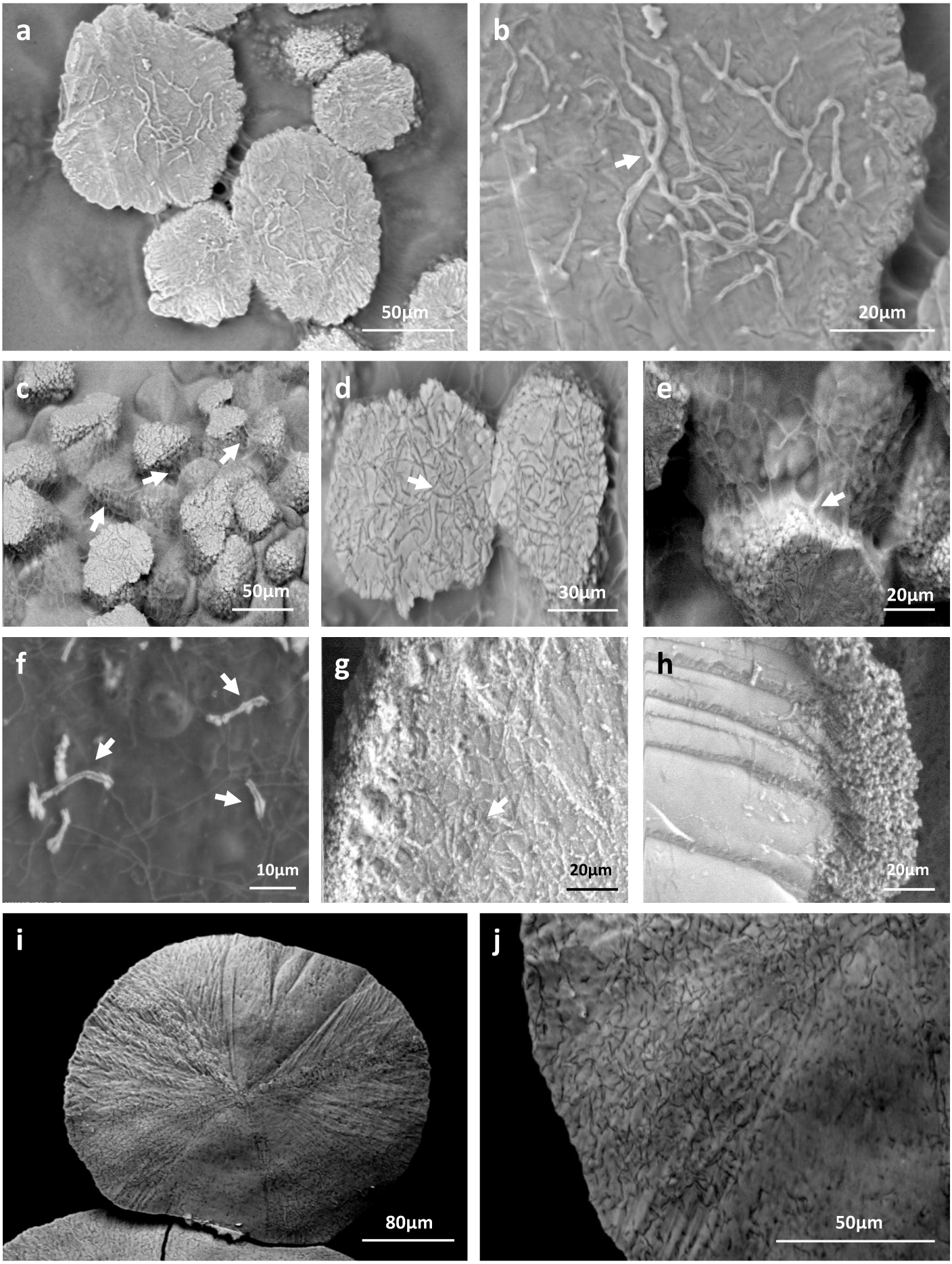
a
50µm
b
20µm
c
50µm
d
30µm
e
20µm
f
10µm
g
20µm
h
20µm
i
80µm
j
50µm

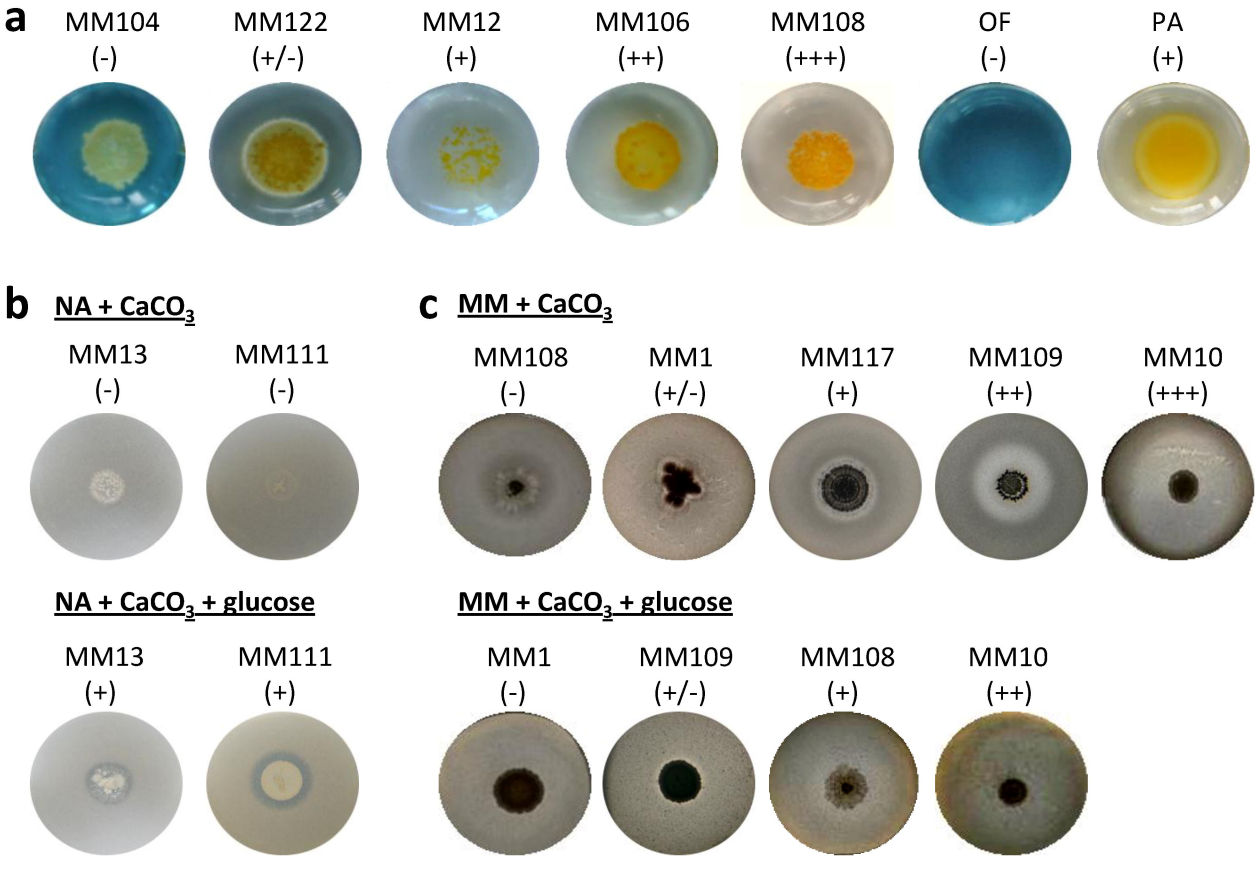
a
MM104
(-)
MM122
(+/-)
MM12
(+)
MM106
(++)
MM108
(+++)
OF
(-)
PA
(+)
b
NA + CaCO3
MM13
(-)
MM111
(-)
NA + CaCO3 + glucose
MM13
(+)
MM111
(+)
c
MM + CaCO3
MM108
(-)
MM1
(+/-)
MM117
(+)
MM109
(++)
MM10
(+++)
MM + CaCO3 + glucose
MM1
(-)
MM109
(+/-)
MM108
(+)
MM10
(++)

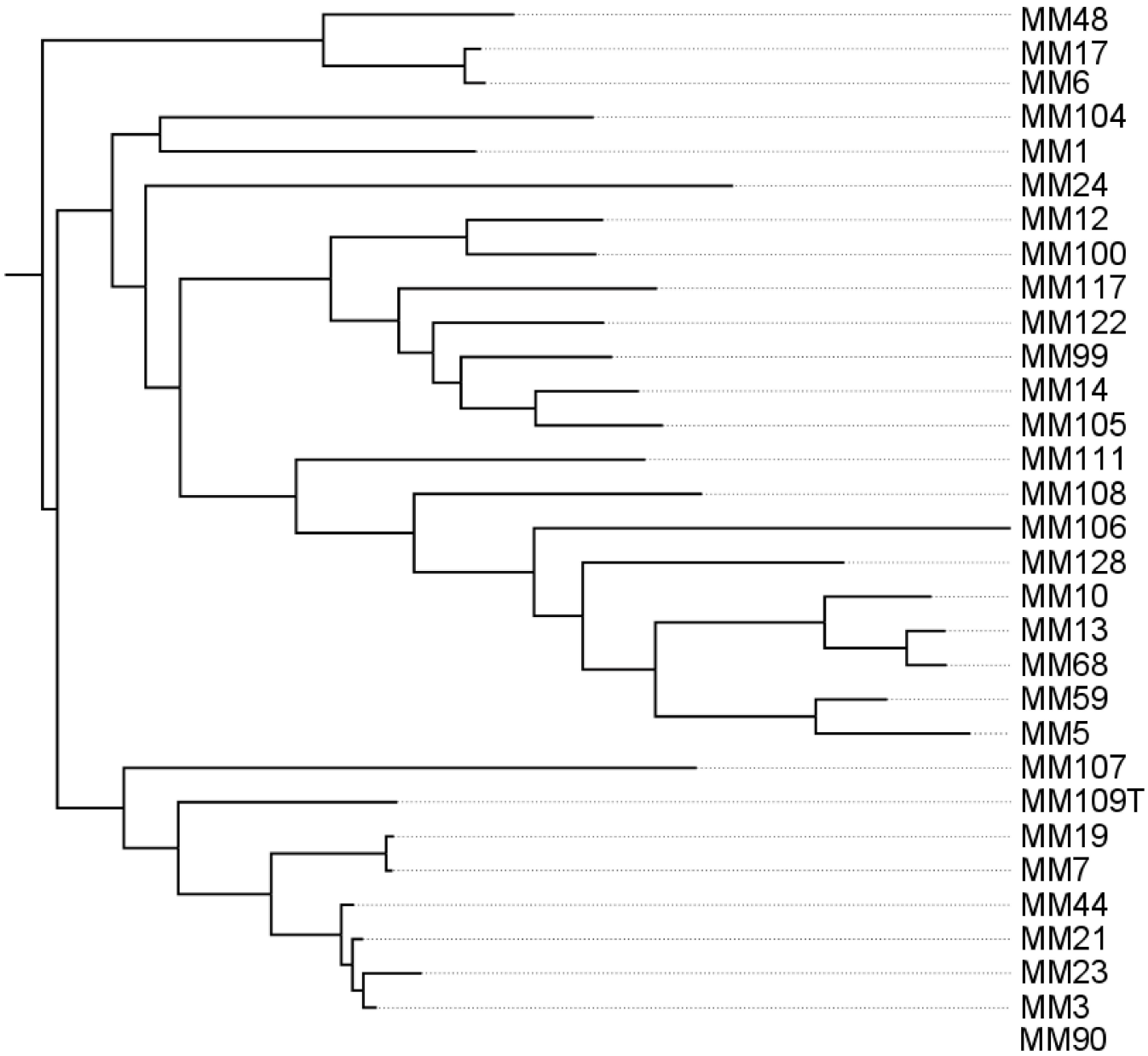

O	MM	MMg	NA	NAg
4	4	1	0	0
0	4	0	0	0
0	4	0	0	0
0	2	0	0	0
0	1	0	0	0
4	1	0	0	0
2	0	0	0	0
0	2	0	0	0
4	2	0	0	0
1	2	0	0	0
0	3	0	0	0
4	3	1	0	0
4	2	0	0	1
4	1	2	0	2
4	0	2	0	0
3	0	0	0	0
2	4	3	0	1
2	4	3	0	0
4	0	0	0	1
4	4	3	0	1
0	3	0	0	0
0	3	0	0	0
0	1	0	0	0
4	3	1	0	0
0	0	0	0	0
3	4	0	0	0
4	1	0	0	1
4	3	0	0	0
1	0	1	0	1
4	3	0	0	0
3	2	0	0	1